

University of Windsor

Scholarship at UWindor

Electronic Theses and Dissertations

Theses, Dissertations, and Major Papers

2016

Bis(benzimidazolium) Rotaxane Molecular Shuttles

Christine To

University of Windsor

Follow this and additional works at: <https://scholar.uwindsor.ca/etd>

Recommended Citation

To, Christine, "Bis(benzimidazolium) Rotaxane Molecular Shuttles" (2016). *Electronic Theses and Dissertations*. 5779.

<https://scholar.uwindsor.ca/etd/5779>

This online database contains the full-text of PhD dissertations and Masters' theses of University of Windsor students from 1954 forward. These documents are made available for personal study and research purposes only, in accordance with the Canadian Copyright Act and the Creative Commons license—CC BY-NC-ND (Attribution, Non-Commercial, No Derivative Works). Under this license, works must always be attributed to the copyright holder (original author), cannot be used for any commercial purposes, and may not be altered. Any other use would require the permission of the copyright holder. Students may inquire about withdrawing their dissertation and/or thesis from this database. For additional inquiries, please contact the repository administrator via email (scholarship@uwindsor.ca) or by telephone at 519-253-3000ext. 3208.

Bis(benzimidazolium) Rotaxane

Molecular Shuttles

By

Christine To

A Thesis
Submitted to the Faculty of Graduate Studies
through the Department of Chemistry and Biochemistry
in Partial Fulfillment of the Requirements for
the Degree of Master of Science at
The University of Windsor

Windsor, Ontario, Canada

© 2016 Christine To

Bis(benzimidazolium) Rotaxane Molecular Shuttles

by

Christine To

APPROVED BY:

J. Ciborowski
Department of Biological Sciences

C. Macdonald
Department of Chemistry and Biochemistry

S. Loeb, Advisor
Department of Chemistry and Biochemistry

June 17, 2016

Declaration of Co-authorship

I hereby declare that this thesis incorporates material that is result of joint research as follows: Project design was developed by Dr. Stephen Loeb and Dr. Nicholas Vukotic. Synthetic experiments were designed by the author with additional input given by Dr. Kelong Zhu and Dr. Nicholas Vukotic. All experiments and characterization were conducted by the author with the exception of single crystal X-ray diffraction experiments which were conducted by Pablo Martinez Bulit and Dr. Kelong Zhu.

I am aware of the University of Windsor Senate Policy on Authorship and I certify that I have properly acknowledged the contribution of other researchers to my thesis, and have obtained written permission from each of the co-author(s) to include the above material(s) in my thesis.

I certify that, with the above qualification, this thesis, and the research to which it refers, is the product of my own work.

I certify that, to the best of my knowledge, my thesis does not infringe upon anyone's copyright nor violate any proprietary rights and that any ideas, techniques, quotations, or any other material from the work of other people included in my thesis, published or otherwise, are fully acknowledged in accordance with the standard referencing practices. Furthermore, to the extent that I have included copyrighted material that surpasses the bounds of fair dealing within the meaning of the Canada Copyright Act, I certify that I have obtained a written permission from the copyright

owner(s) to include such material(s) in my thesis and have included copies of such copyright clearances to my appendix.

I declare that this is a true copy of my thesis, including any final revisions, as approved by my thesis committee and the Graduate Studies office, and that this thesis has not been submitted for a higher degree to any other university or institution.

Abstract

Rotaxanes are Mechanically Interlocked Molecules (MIMs) formed by a dumbbell-shaped axle and a macrocyclic wheel, which cannot be separated without breaking a covalent bond. Incorporation of rotaxanes into Metal-Organic Frameworks (MOFs) produces organized, dense solid-state systems. This thesis describes the synthesis and study of novel [2] and [3]bis(benzimidazolium) rotaxanes, including shuttling studies and MOF synthesis.

Chapter 1 provides an introduction to MIMs and molecular shuttling, in solution and solid-state. The idea of incorporating MIMs into MOFs is addressed.

Chapter 2 describes the synthesis of two new rotaxanes as well as preliminary study of a cucurbit[7]uril [2]pseudorotaxane. Shuttling studies of the [2]rotaxane in solution were conducted. MOF synthesis incorporating both the [2] and [3]rotaxanes as linkers and analysis of PXRD patterns to determine the probable structures of the MOFs. Finally, summary and possible future work are described.

Chapter 3 describes all of the experimental details including the full synthetic procedure for the preparation of [2] and [3]rotaxanes and relevant characterisation data.

Acknowledgements

I would like to thank Dr. Stephen Loeb for allowing me to work in his research group since my second year of undergraduate studies at the University of Windsor. Through the years, he has proven to be incredibly supportive, understanding and motivating in every situation. He has contributed greatly not only to my success as a chemist but also my personal development through the years.

I would also like to thank my fellow Loeb group members, past and present. They have always provided me with support through the good and bad times of chemistry (and life). I would like to thank Dr. Nick Vukotic for teaching me everything about synthetic chemistry since I started with the Loeb Research group and inspiring and motivating me through the years. I would also like to thank Dr. Kelong Zhu for his incredible advice, assistance and patience for the duration of my Master's degree. Furthermore, I would like to thank Pablo Martinez Bulit who, in conjunction with Kelong, worked tirelessly on the Single Crystal X-ray diffractometer and when solving crystal structures for me.

Finally, I'd like to thank my friends and family who have supported me through my entire chemistry career. Most notably, Emilyn Anderi for taking on this journey with me and being my source of support and giggles through the years. Finally, my parents, although unacquainted with what I actually do in the lab, have been incredibly supportive and understanding of my late nights and many hours away from home dedicated to Chemistry.

Table of Contents

Declaration of Co-authorship.....	iii
Abstract	v
Acknowledgements.....	vi
List of Tables	ix
List of Figures	x
List of Abbreviations	xv
Chapter 1 – Mechanically Interlocked Molecules.....	1
1.1 Introduction	1
1.2 Mechanically Interlocked Molecules	1
1.2.1 Pseudorotaxanes and Rotaxanes	2
1.3 Molecular Machines.....	5
1.3.1 Molecular Shuttles and Molecular Switches	5
1.4 Metal-Organic Frameworks.....	9
1.4.1 Introduction.....	9
1.4.2 Metal Organic Rotaxane Framework.....	10
1.4.3 Cucurbit[n]uril Polyrotaxane Frameworks.....	13
1.4.4 Dynamics in Metal Organic Rotaxane Framework	16
1.5 Scope of Thesis	18
Chapter 2 – Results and Discussion	22
2.1 Organic Synthesis	22
2.2 Determination of Shuttling Rate of [2]Rotaxane.....	32
2.3 CB[7] [2]Pseudorotaxane	37
2.4 Single-Crystal X-Ray Structures	40
2.4.1 [2]Rotaxane and [3]Rotaxane	40
2.4.2 MOF Synthesis	47
2.4.3 [2]Rotaxane and [3]Rotaxane MOFs.....	50
2.5 Powder X-Ray Diffraction.....	51
2.6 Summary and Future Work.....	55
Chapter 3 - Experimental.....	57
3.1 General Comments.....	57

3.2 Synthesis of 1 and [1-H ₂][BF ₄] ₂	58
3.3 Synthesis of 2, Pentaethyleneglycol-dipent-4-enyl ether	60
3.4 Synthesis of 3a and 3b	62
3.5 Synthesis of 4a and 4b	64
3.6 Synthesis of 5a and 5b.....	67
3.7 Synthesis of Benzoic Acid Terminated Bis(benzimidazole) Axle	69
References	70
Appendix	76
Vita Auctoris	86

List of Tables

Table 1. Summary of Percent Yield and Rotaxane Ratio ([2]:[3])	25
Table 2. Comparison of Benzo-bis(imidazolium) [2]Rotaxane and Bis(benzimidazolium) [2]Rotaxane Shuttling Rates and Thermodynamic Parameters at 298K.	36
Table 3. Crystal Data and Solution Results for Tetraester [3]Rotaxane, 4b	46
Table 4. MOF Synthesis Trials with Tetraacid [2]Rotaxane (5a)	48
Table 5. MOF Synthesis Trials with Tetraacid [3]Rotaxane (5b).	48

List of Figures

Figure 1. Schematic diagrams of a.) catenane b.) Borromean rings and c.) rotaxane...	1
Figure 2. a.) [24]-Crown-6-ether wheel b) dibenzo-[24]-crown-8 ether wheel.....	2
Figure 3. Schematic example of a [2]pseudorotaxane showing the non-covalent interactions between the triphenylimidazolium axle and the benzo crown ether wheel.	3
Figure 4. Schematic diagram showing: a.) [2]pseudorotaxane formation by threading of the axle (blue) with macrocyclic wheel (red) and b.) capping with bulky stoppering groups (green) to form [2]rotaxane.	4
Figure 5. Schematic diagram of the clipping method for [2]rotaxane formation. The dumbbell shaped axle is represented in blue and the macrocycle is in red.....	4
Figure 6. H-shaped bis(benzimidazolium) [2]rotaxane which can function as a molecular shuttle with different macrocyclic crown ether wheels represented by the red ring. Some of the macrocycles studied include 24C8, DB24C8 and DN24C8 ether wheels.....	6
Figure 7. A bistable [2]rotaxane molecular shuttle. The electro-poor cyclophane macrocycle (blue) is able to shuttle between the benzidine and biphenol stations on the axle (red) through acid-base chemistry.	7
Figure 8. Left: MOF-5 structure which shows ZnO ₄ tetrahedra (blue tetrahedral) joined by benzene dicarboxylate ligands. ¹⁹ Right: HKUST-1 which consists of dimeric cupric tetracarboxylate units from the benzene-1,3,5-tricarboxylate and axial aquo ligands. ²⁰	9
Figure 9. a.) Dipyridinium [2]pseudorotaxane threaded with DB24C8, 9a and b.) analogous N-oxide dibipyridinium [2]pseudorotaxane threaded with DB24C8, 9b	10
Figure 10. a.) 2D square grid obtained from reaction of 9a with [Cd(H ₂ O) ₆][BF ₄] ₂ in MeNO ₂ b.) 2D MORF obtained from reaction of 9b with [Cd ^{II}][OTf] ₂	11
Figure 11. 3D polyrotaxane framework formed from reaction of 9b with [Sm ^{III}][OTf] ₃ . Left image shows the framework without macrocycles and right image shows framework with macrocycles. ²⁵	12
Figure 12. Line drawing of cucurbit[n]uril.	13

Figure 13. a.) 3-pyridyl diaminobutane pseudorotaxane PR43 ²⁺ b.) 2d polyrotaxane network formed from reaction of PR4 ²⁺ and silver nitrate c.) 3-pyridyl diaminopentane pseudorotaxane PR53 ²⁺ d.) helical 2D polyrotaxane formed from the reaction of PR53 ²⁺ and silver	15
Figure 14. a.) 3-Phenyl carboxylate diaminobutane pseudorotaxane PCA43 ²⁺ b.) 3D polyrotaxane network formed by reaction with Tb(NO ₃) ₃ . CB is represented schematically with ellipses. ²⁸	15
Figure 15. a.) Anilinium rotaxane ligand used in UWDM-1, b.) ball-and-stick representation obtained from single-crystal x-ray diffraction of the polyhedral cavities viewed down c-axis with macrocyclic rings omitted and with macrocyclic rings, b and c, respectively. ¹¹	16
Figure 16. H-Shaped [2]rotaxane shuttle ligand used in MOF UWDM-4.....	18
Figure 17. Left: Benzo-bisimidazolium axle core. Right: Bis(benzimidazolium) axle core	19
Figure 18. Target [2] and [3]bis(benzimidazolium) rotaxanes	19
Figure 19. Isophthalate C ₅ distance comparison between a.) benzo-bis(imidazolium) [2]rotaxane b.) target bis(benzimidazolium) [2]rotaxane and c.) pentaphenyl tetraacid ligands.	21
Figure 20. Top: ¹ H NMR spectrum of tetraester [3]rotaxane, 4b and Bottom: ¹ H NMR spectrum of tetraester [2]rotaxane, 4a	26
Figure 21. Full ROESY Spectrum of tetraester [2]rotaxane, 4b . (CDCl ₃ at 500 MHz). 28	
Figure 22. Tetraester [2]rotaxane (4b) proton environments.....	28
Figure 23. Cross-section of aromatic (f1) and NH (f2) regions in ROESY of 4b (CDCl ₃ at 500 MHz)	29
Figure 24. Cross-section of macrocycle (f1) and aromatic (f1) regions in ROESY of 4b (CDCl ₃ at 500 MHz)	30
Figure 25. Cross-section of macrocyclic regions (f1) and (f2) in ROESY of 4b (CDCl ₃ at 500 MHz)	30
Figure 26. Cross-section of aromatic region (f1) and NH region (f2) in ROESY of 4b (CDCl ₃ at 500 MHz)	31

Figure 27. Shuttling states of [2]rotaxane and benzimidazolium proton environment studied via VT ^1H NMR.	32
Figure 28. Benzimidazole N-H and aromatic regions of variable temperature ^1H NMR of [2]Rotaxane, 5a (500 MHz in CD_3CN).....	33
Figure 29. Experimental and Simulated VT ^1H NMR spectrum of 4b	34
Figure 30. Eyring Plot of shuttling rates of 4b	35
Figure 31. ^1H NMR spectra of a.) CB[7] b.) 3,3'-diamino benzidine c.) inclusion complex of CB[7] and 3,3'-benzidine in 0.1M D_2SO_4 in D_2O at 500 MHz.	37
Figure 32. ^1H NMR of [2]pseudorotaxane formation and uncomplexed CB[7] in 0.1M D_2SO_4 in D_2O at 500 MHz.	38
Figure 33. Left: Physical appearance of tetraester [2]rotaxane (4a) obtained from slow diffusion of MeOH vapour into a solution of 4a in DMF. Crystals (small needles of 0.01 mm) are viewed under polarized light for better visualization. Right: physical appearance crystals (blocks of 0.20-0.40mm) of tetraester [3]rotaxane (4b) obtained from slow diffusion of hexanes into a solution of 4b in CHCl_3	40
Figure 34. Ball-and-stick representations of X-ray crystal structure of tetraester [3]rotaxane, 4b . Labeling scheme is black = carbon, blue = nitrogen red = oxygen, green = fluorine, yellow = boron. Left: View perpendicular to axle plane, Right: view along axle plane with counterions omitted for clarity. Solvent molecules omitted for clarity in both representations..	41
Figure 35. Space-filling diagram of tetraester [3]rotaxane, 4b . Labeling Scheme is blue = axle, white = axle oxygens, red = wheel, yellow = boron, green = fluorine. Solvent molecules are omitted for clarity.	42
Figure 36. Ball-and-stick representations of X-ray crystal Structure of tetraester [3]rotaxane (4b) showing hydrogen bonding interactions between axle imidazole and wheel oxygens shown with yellow dashed line. Protons not involved in hydrogen bonding are removed for clarity. Labeling scheme: blue = axle, red = wheel. yellow = boron, green = fluorine. Solvent molecules are omitted for clarity.....	42
Figure 37. Ball-and-stick representation of π -stacking interactions between [3]rotaxane with π -stacking distance represented by yellow dashed line. Hydrogen	

atoms, counter ions and solvent molecules omitted for clarity. Labelling scheme: axle = blue, wheel = red.	44
Figure 38. Space-filling representation of [3]rotaxane packing. Labelling scheme: axle = blue, wheel = red, oxygen = white. Counter ions and solvent molecules omitted for clarity.....	44
Figure 39. Space-filling representation of packing of [3]rotaxane between solvent and counterion layer. Labelling Scheme: Blue = axle, red = wheel, dark green = flourine, yellow = boron, light green = CHCl ₃ carbon, neon green = chlorine.	45
Figure 40. Space-filling representation of [3]rotaxane packing between solvent and counterion layer along c-axis. Labelling scheme: Blue = axle, red = wheel, dark green = flourine, yellow = boron, light green = CHCl ₃ carbon, neon green = chlorine.	45
Figure 41. [2]Rotaxane MOF crystals obtained from the reaction of tetraacid[2]rotaxane, 5a with Cu(NO ₃) ₂ •2.5H ₂ O through solvothermal synthesis with a.) a solvent system of 2:1:1 DEF:EtOH:H ₂ O in Trial 1 b.) a solvent system of 4:1:1 DEF:EtOH:H ₂ O in Trial 2.....	50
Figure 42. [3]Rotaxane MOF crystals obtained from reaction of tetraacid [3]rotaxane, 5b , with Cu(NO ₃) ₂ •2.5H ₂ O through solvothermal synthesis with a solvent system of 1:1:0.5 DMF:1,4-Dioxane:H ₂ O	51
Figure 43. The physical appearance of cubic crystals obtained the reaction of tetraacid benzo-bis(imidazolium) [2]rotaxane and Cu(II) metal.....	51
Figure 44. PXRD pattern of [2]rotaxane 5a MOF synthesis Trial 1 (red) and Trial 2 (black). Trial 1 resulted in the formation of a mixture of aggregate and cubic crystals meanwhile Trial 2 resulted in the formation of uniform cubic crystals.	52
Figure 45. Experimental PXRD patterns of UWCM-2 (blue), [2]rotaxane MOF (black), [3]rotaxane MOF (red) and simulated PXRD pattern of NOTT-104 (green).	53
Figure 46. Ball-and-stick representation of the cubic cavity within the framework. Macrocycles are omitted for clarity. The rotaxanes coordinate to dimeric Cu ^{II} paddlewheels which self-assemble into cubooctahedral cages (nanoballs). The yellow sphere represents the solvent accessible space within the MOF. ³⁷	54
Figure 47. Chemical structure and proton environments of 1	58
Figure 48. Structure and proton environments of [1 -H ₂][BF ₄] ₂	58

Figure 49. Synthetic pathway, structure and proton environments of Pentaethyleneglycol-dipent-4-enyl ether.	60
Figure 50. Structure and proton environments of 3a	63
Figure 51. Structure and proton environments of 3b	63
Figure 52. Structure and proton environments of 4a	64
Figure 53. Structure and proton environment of 4b	65
Figure 54. Structure and proton environment of 5a	67
Figure 55. Structure and proton environments of 5b	68
Figure 56. Structure and proton environments of benzoic acid terminated bis(benzimidazolium) axle.	69

List of Abbreviations

CB	Cucurbituril
d	Doublet
DB	Dibenzo
DCM	Dichloromethane
DEF	Diethylformamide
DMF	Dimethylformamide
EtOH	Ethanol
Et₂O	Diethyl Ether
EtAcO	Ethyl Acetate
EXSY	Exchange Spectroscopy
g	gram
Hz	Hertz
h	Hour(s)
m	Multiplet
MeOH	Methanol
mg	Milligram
MHz	Megahertz
MIM	Mechanically-Interlocked Molecule
mmol	Millimole
mL	Millilitre
MOF	Metal-Organic Framework

MORF	Metal-Organic Rotaxane Framework
M.P.	Melting Point
NMR	Nuclear Magnetic Resonance
NOESY	Nuclear Overhauser Effect Spectroscopy
Ph	Phenyl
PRF	Polyrotaxane Framework
PXRD	Powder X-ray Diffraction
q	Quartet
ROESY	Rotational-Frame Nuclear Overhauser Effect Correlation Spectroscopy
RT	Room Temperature
s	Singlet
SBU	Secondary Building Unit
SS	Solid-State
TFA	Trifluoroacetic Acid
THF	Tetrahydrofuran
TLC	Thin-Layer Chromatography
VT	Variable Temperature

Chapter 1 – Mechanically Interlocked Molecules

1.1 Introduction

Mechanically Interlocked Molecules (MIMs) are of particular interest in supramolecular chemistry because of the potential to control and manipulate the relative motions of the component molecules. With the application of external stimuli, this has been successfully accomplished through the synthesis of molecular shuttles¹⁻³, molecular switches⁴⁻⁶ and molecular machines⁷. Molecular shuttles and molecular switches contain at least two stable states for which the component molecules can exist. Molecular machines are defined as molecules that are able to perform mechanical movement or a net positional displacement.⁸

1.2 Mechanically Interlocked Molecules

Mechanically interlocked molecules are defined by the inability to separate component molecules without the breaking of covalent bonds. Some examples of mechanically interlocked molecules include catenanes, Borromean rings, and rotaxanes (**Figure 1**). Their formation is driven primarily by non-covalent interactions between the component molecules and involves a synthetic 'trapping' step.

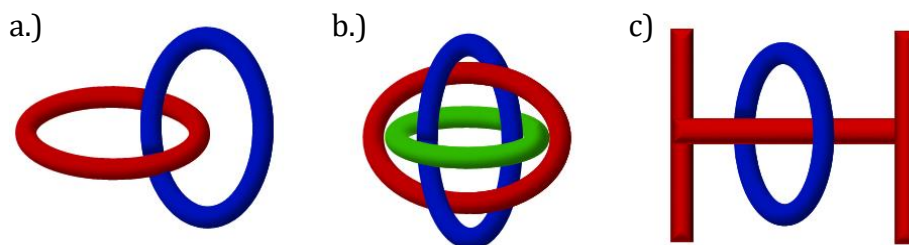


Figure 1. Schematic diagrams of a.) catenane b.) Borromean rings and c.) rotaxane.

Some of the most prominently studied supramolecular systems are pseudorotaxanes and rotaxanes. The component molecules of a rotaxane are the dumbbell-shaped “axle” and macrocyclic “wheel”. Crown ethers are one example of a macrocyclic wheel used in rotaxane formation. **Figure 2** shows two examples of crown ether wheels, [24]crown-6 and dibenzo-[24]crown-8, which can be abbreviated as 18C6 and DB24C8, respectively. The integer prefix indicates the number of atoms, including heteroatoms, in the ring and the postfix number indicate the number of heteroatoms.

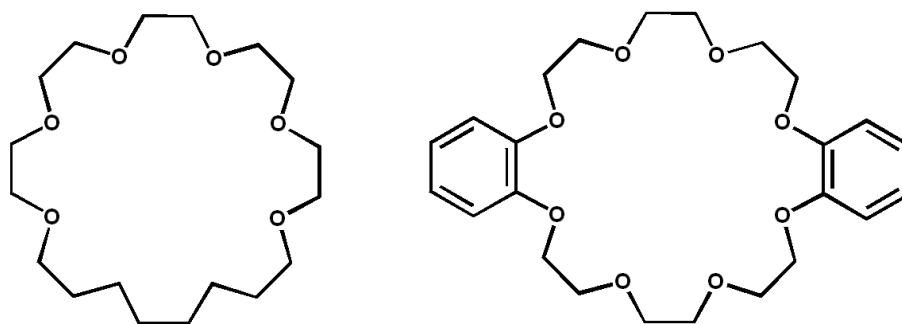


Figure 2. a.) [24]-Crown-6-ether wheel b) dibenzo-[24]-crown-8 ether wheel.

The number of components in a rotaxane is designated by a bracketed integer prefix (e.g. [2]rotaxane). Furthermore the prefix ‘pseudo-’ is used to describe when the complementary components are interpenetrated or not permanently interlocked but in equilibrium with their individual components.

1.2.1 Pseudorotaxanes and Rotaxanes

These supramolecular assemblies are of particular interest to chemists because of the possibility of synthesizing interlocked molecules and coordination polymers with advanced structural complexity. Pseudorotaxanes are formed through non-covalent interactions between the axle and the wheel. In a pseudorotaxane, these

components are in equilibrium between the associated and 'unthreaded' species. Thus, the ability to 'trap' the macrocyclic wheel to form a rotaxane is necessary to form an interlocked species.

Figure 3 depicts an example of a [2]pseudorotaxane which is comprised of a triphenylimidazolium axle and a dibenzo-[24]-crown-8 wheel.⁹ In this example, non-covalent interactions like hydrogen-bonding, π -stacking, and ion-dipole interactions allow the axle to 'thread' into the wheel to form an interpenetrated species.

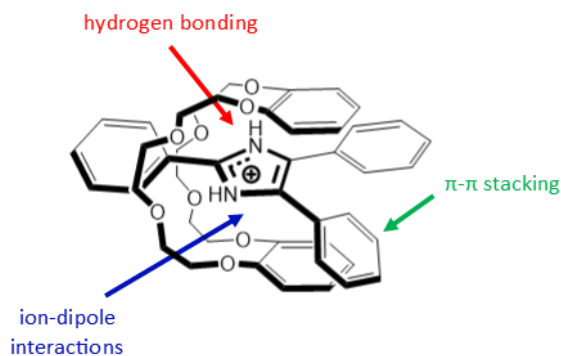


Figure 3. Schematic example of a [2]pseudorotaxane showing the non-covalent interactions between the triphenylimidazolium axle and the benzo crown ether wheel.

In order to form an interlocked rotaxane molecule, the unthreading of the macrocycle must be prevented with bulky stoppering groups. This can be achieved through many synthetic methods, however the two most common methods of rotaxane formation are capping a pseudorotaxane with bulky groups or clipping of the macrocyclic wheel onto a dumbbell shaped axle.¹⁰ In the capping method, a pseudorotaxane is formed through the threading of the axle and wheel. As seen in **Figure 4a** these components are not permanently interlocked and exists in an equilibrium of associated and non-associated species. This is then followed by attachment of bulky end groups to form an interlocked species (**Figure 4b**).

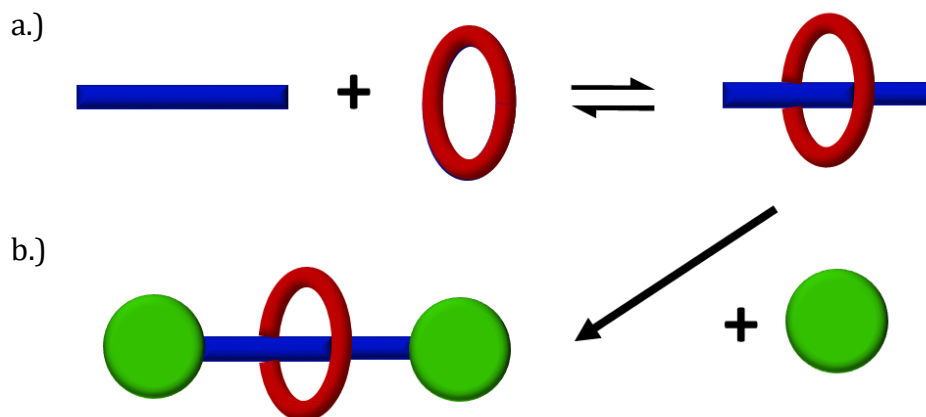


Figure 4. Schematic diagram showing: a.) [2]pseudorotaxane formation by threading of the axle (blue) with macrocyclic wheel (red) and b.) capping with bulky stoppering groups (green) to form [2]rotaxane.

Alternatively, in the clipping method an open macrocyclic wheel unit is formed around a dumbbell shaped axle through a ring closing reaction to form a rotaxane (**Figure 5**). This method utilizes template-directed synthesis which requires an appropriate recognition site for the open wheel component to interact with before ring closing is performed. Some recognition sites previously studied in the Loeb research group include a benzyl-anilinium¹¹, bis(pyridinium)ethane¹² and benz(imidazolium) groups.² For a crown ether wheel, ring closing metathesis can be conducted using Grubb's I catalyst followed by reduction of the olefin.¹¹

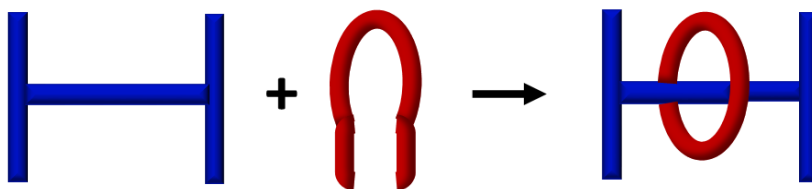


Figure 5. Schematic diagram of the clipping method for [2]rotaxane formation. The dumbbell shaped axle is represented in blue and the macrocycle is in red.

1.3 Molecular Machines

Molecular machines are defined as molecules that are able to perform mechanical movement or a net positional displacement.⁸ In order to function as a molecular machine, the manipulation and control of the components is necessary. Therefore, rotaxanes have become the ideal candidate for the synthesis of molecular machines because of their interlocked nature and tunability. Furthermore, it has been demonstrated that the application of external stimuli is able to induce movement of the macrocycles to function as molecular switches.

1.3.1 Molecular Shuttles and Molecular Switches

The ability to switch between different translational co-conformations has been successfully accomplished through the synthesis of [2]rotaxanes molecular shuttles.¹³ This is possible through the presence of two distinct recognition sites between which the wheel is able to shuttle. If the two recognition sites possess the same binding affinity to the macrocycle, the sites are degenerate and the ring will spend equal amounts of time on either site. However, when the recognition sites have different binding affinities, this introduces the possibility of creating a bistable rotaxane. This creates binary states of “0” and “1” in which the rotaxane can exist.

In molecular shuttles with degenerate sites, the shuttling rate can be affected by the interactions between the templating components. For example, in the Loeb research group a bis(benzimidazolium) axle was able to form molecular shuttles with two degenerate sites using various crown ether wheels.^{2,14}

Figure 6 shows a rigid H-shaped [2]rotaxane which was shown to function as a molecular shuttle containing macrocyclic crown ethers of varying sizes and shapes. This rotaxane is synthesized through first forming the [2]pseudorotaxane followed by capping to form the interlocked [2]rotaxane. Determination of association constants of the pseudorotaxane through variable temperature (VT) ^1NMR studies in CD_3CN showed a correlation between the strength of interaction between the axle and wheel and yield of rotaxane formation. This is because the stronger the non-covalent interactions between the complementary components, the larger the barrier required to break interactions to shuttle from one site to another. ²

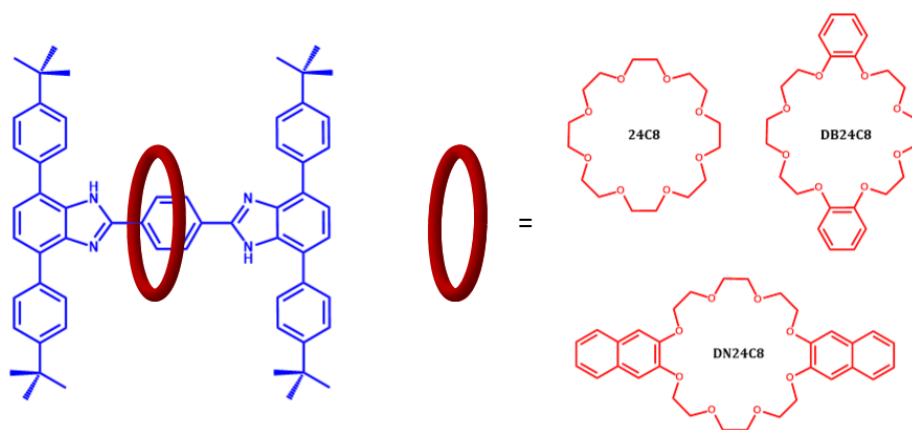


Figure 6. H-shaped bis(benzimidazolium) [2]rotaxane which can function as a molecular shuttle with different macrocyclic crown ether wheels represented by the red ring. Some of the macrocycles studied include 24C8, DB24C8 and DN24C8 ether wheels.

Rotaxanes with non-degenerate states can form molecular switches if the position of the macrocycle is able to be reversibly controlled by a stimulus. The position of the macrocyclic wheel can be manipulated between co-conformations by chemical,¹⁵ electrochemical¹⁶ or photochemical^{17,18} stimuli.

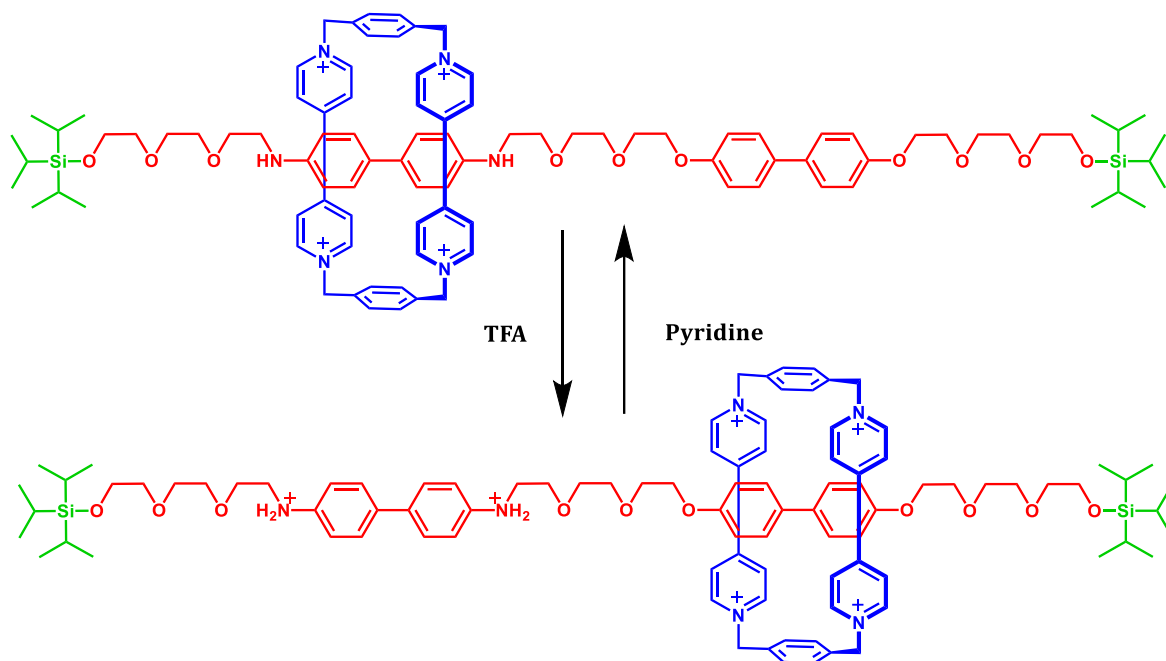


Figure 7. A bistable [2]rotaxane molecular shuttle. The electro-poor cyclophane macrocycle (blue) is able to shuttle between the benzidine and biphenol stations on the axle (red) through acid-base chemistry.

The first bistable [2]rotaxane switchable molecule shuttle was reported by Stoddart, Kaifer, and co-workers in 1994. This rotaxane consists of two different π -electron donating stations and a π -accepting tetracationic cyclophane which consists of two bipyridinium units bridged by p-xylyl spacers. The axle, in red, consists of benzidine and biphenol units within a polyether chain terminated by bulky triisopropyl siloxane groups as stoppers in green. The position of the wheel can be switched from one site to another by acid-base chemistry or electrochemical oxidation of the benzidine station. **Figure 7** depicts the shuttling of the wheel with the addition of acid or base. With the addition of trifluoroacetic acid (TFA) the benzidine site becomes protonated and causes unfavourable electrostatic repulsion with the tetracationic wheel and induces shuttling to the biphenol station. The addition of pyridine deprotonates the benzidine station and reverses the translational movement.

This shuttling movement was studied through ^1H NMR spectroscopy and considerable upfield shifts of the proton environments of the biphenol station were observed upon addition of deuterated trifluoroacetic acid in comparison to biphenol in free axle. This is indicative of the shielding effect caused by the shutting of the wheel to this station. Furthermore, neutralization with pyridine causes a regeneration of the spectrum obtained before addition of acid. This demonstrates the reversible nature of the translational motion. The shuttling was also confirmed by room-temperature (RT) UV/visible spectroscopy. Previously, it had been shown that the benzidine derivative is able to form a green charge-transfer complex with the cyclophane ($\lambda_{\text{max}} = 690 \text{ nm}$), whereas the biphenol species produces a red complex ($\lambda_{\text{max}} = 480 \text{ nm}$). The decrease in absorption at 690 nm upon the addition of TFA is indicative of the shutting of the wheel. Moreover, electrochemical oxidation of the benzidine station was studied through cyclic voltammetry. It showed that the wheel affects the first one-electron oxidation of the benzidine subunit but not the second because the development of the positive charge causes the wheel to shuttle to the biphenol station.¹⁶

1.4 Metal-Organic Frameworks

1.4.1 Introduction

Metal Organic Frameworks (MOFs) are porous coordination networks formed by organic ligands and inorganic clusters known as secondary building units (SBUs).¹⁵

Figure 8 shows archetypal MOFs: MOF-5, the first MOF to use ZnO_4 clusters as SBUs and benzene dicarboxylate ligands¹⁹ and HKUST-1 which utilizes cupric dimers and benzene-1,3,5-tricarboxylate units as ligands.²⁰

MOF-5 consists of $\text{Zn}_4\text{O}(\text{CO}_2)_6$ units which contain four ZnO_4 tetrahedra that join at a common vertex and 6 carboxylate carbon atoms that define the octahedral SBU. The yellow sphere within the centre represents the largest spherical space that can occupy the unit cell without contacting the other organic molecules. This void space has been one of the main driving forces for the increased interest in the synthesis of novel MOF structures. Alternatively, HKUST-1 observes a dicopper(II) tetracarboxylate SBU; this type of dinuclear metal cluster is commonly referred to as a copper “paddle-wheel”.²¹ The paddlewheel subunits are dinuclear metal clusters in

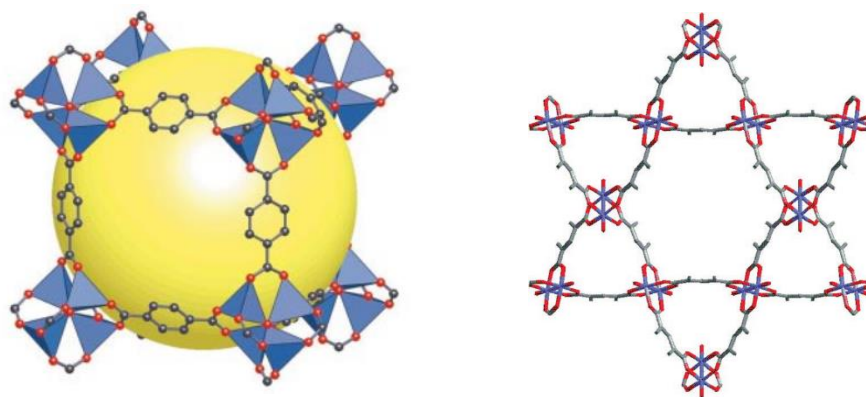


Figure 8. Left: MOF-5 structure which shows ZnO_4 tetrahedra (blue tetrahedral) joined by benzene dicarboxylate ligands.¹⁹ Right: HKUST-1 which consists of dimeric cupric tetracarboxylate units from the benzene-1,3,5-tricarboxylate and axial aquo ligands.²⁰

which the two metals are bridged by four carboxylate groups. The aforementioned SBUs are only 2 of the many of possible building blocks used in the synthesis of MOFs.

Carboxylate frameworks are of particular interest because of the strong metal-carboxylate interactions. With the knowledge of the structure of SBUs, one can perform modular chemistry when taking into consideration the ligand coordinating groups and metals used.²²

1.4.2 Metal Organic Rotaxane Framework

The highly organized and porous structures of MOF can be further modified with the use of rotaxanes as ligands to form Metal-Organic Rotaxane Frameworks (MORFs) sometimes called Polyrotaxane Frameworks (PRFs). The use of rotaxanes as ligands introduces an additional complexity to the ligand used that can be modified in order to obtain unique topologies. Rotaxanes are also able to form one- two-, or three-periodic coordination polymers.¹⁸ Those of particular interest are three-periodic coordination polymers because of the highly dense material that results.

Loeb and coworkers have demonstrated the tunability of using rotaxanes as ligands to obtain unique topologies using the [2]pseudorotaxane ligands²³⁻²⁵ shown in

Figure 9.

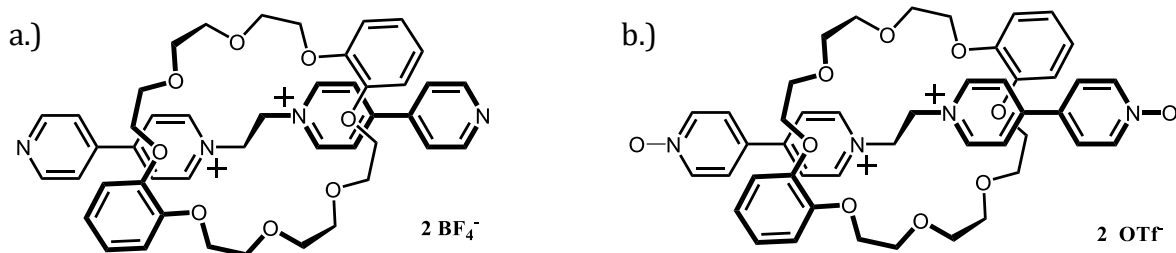


Figure 9. a.) Dipyrrolium [2]pseudorotaxane threaded with DB24C8, **9a** and b.) analogous N-oxide dipyrrolium [2]pseudorotaxane threaded with DB24C8, **9b**.

Comparable MOF synthesis was conducted with both ligands to observe the different topologies that resulted when reacted with Cd^{II} under similar conditions. The bipyridinium pseudorotaxane, **9a**, formed a 2D square grid by reacting 2 equivalents of ligand, 4 equivalents of DB24C8 and 1 equivalent of $[\text{Cd}(\text{H}_2\text{O})_6][\text{BF}_4]_2$ in MeNO_2 . As shown in **Figure 10**, we can see the macrocycles alternating orientation in order to reduce steric interactions with neighbouring macrocycles and maximize π - π stacking interactions with the axle. The octahedral metal centre is coordinated to 4 pseudorotaxanes to form the 2D grid with the axial positions occupied by H_2O and BF_4 .²⁴ The analogous N-oxide ligand, **9b**, forms a distorted 2D grid which alternates between pseudorotaxane and ‘naked’ axle (not complexed with crown ether wheel) depicted in **Figure 10b**. The metal centre adopts an octahedral geometry with two pseudorotaxanes and two naked axles in the square plane and two triflate anions in the axial positions. Furthermore, these 2D grids were observed to layer in a way that prevented the formation of channels.²³

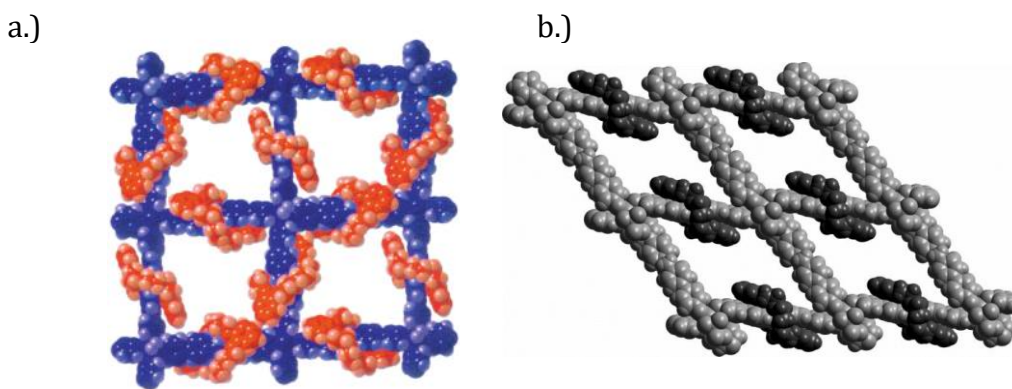


Figure 10. a.) 2D square grid obtained from reaction of **9a** with $[\text{Cd}(\text{H}_2\text{O})_6][\text{BF}_4]_2$ in MeNO_2 b.) 2D MORF obtained from reaction of **9b** with $[\text{Cd}^{\text{III}}][\text{OTF}]_2$.

Further studies using **9b** with lanthanide metals were also conducted in hopes of forming 3D polyrotaxane frameworks. It was thought that the increased ligand length and use of larger lanthanide ions would favour a higher coordination. It was

shown that the reaction of **9b** with Sm^{III}, Eu^{III}, Gd^{III}, and Tb^{III} results in isomorphous 3D polyrotaxanes.

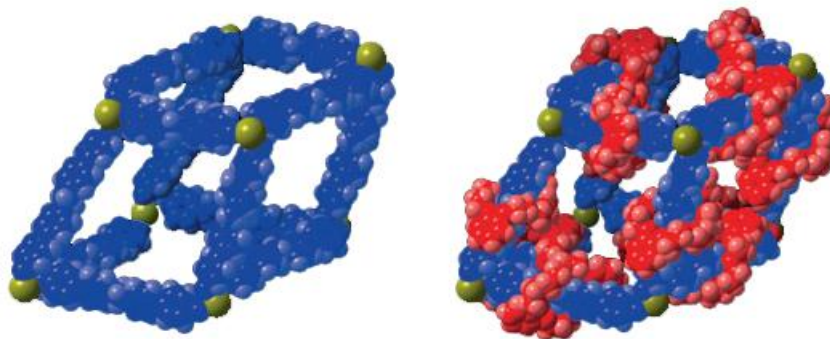


Figure 11. 3D polyrotaxane framework formed from reaction of **9b** with [Sm^{III}][OTf]₃. Left image shows the framework without macrocycles and right image shows framework with macrocycles.²⁵

Shown in **Figure 11** is the 3D polyrotaxane framework formed from reaction of 1 equivalent of **9b**, 3 equivalents of DB24C6 and 1 equivalent of [Sm^{III}][OTf]₃. The rotaxane framework obtained however is interpenetrated by a parallel net. This means that within the void space of one framework, a second framework is interwoven. As predicted, the use of an elongated ligand and larger lanthanide metal allowed for formation of a 3-dimensional framework but also introduced large cavities with a volume of 10,000 Å³ that allowed for the interpenetration of a second net. This highlights just one of the difficulties faced when attempting to synthesize a 3-dimensional metal-organic rotaxane framework.²⁵

1.4.3 Cucurbit[n]uril Polyrotaxane Frameworks

Cucurbiturils are a unique family of macrocycles which consist of units of glycouril linked by methylene groups as seen schematically in **Figure 12**. The number of glycouril units is designated by the number in brackets *i.e.* cucurbit[7]uril which can be abbreviated to CB[7]. These macrocyclic hosts possess a hydrophobic interior and an electron rich outer rim formed by the carbonyl oxygen atoms. Other examples of this type of cage-like macrocyclic structures include cyclodextrins and calixarenes. These macrocycles are able to form host-guest complexes with complementary molecules in which the CB acts as the host. In order for this to occur, the molecules must be compatible with the hydrophobic interior and the size and electrostatics of the portal opening.

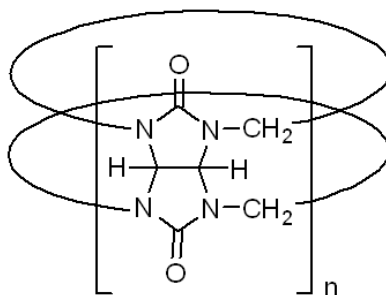


Figure 12. Line drawing of cucurbit[n]uril.

The interaction between CBs and included guests are a results of two types of intermolecular forces: ion-dipole and hydrophobic interactions. Ion-dipole interactions occur between the positive charge of its guest and the carbonyl oxygens of the CB meanwhile the hydrophobic interactions stem from the interaction of the guest and the inner surface of the CB cavity. These interactions are similar to the non-covalent interactions required to trap a macrocycle for the formation of rotaxanes. As a result, CB rotaxanes are of particular interest in the synthesis of novel interlocked

molecules. Furthermore, unlike typical macrocycles like crown ethers, the use of CBs have the ability to impart water solubility to these supramolecular complexes which is particularly applicable in biological systems.²⁶

CB[6] polyrotaxanes have been studied extensively by Kimoon Kim and coworkers. The synthesis involves the threading of a CB[6] 'bead' with a short 'string' to form a pseudorotaxane which is then followed by coordination with metal ions. One of the 'strings' or 'axles' studied consists of a diaminobutane core which has been shown to successfully form inclusion complexes with CB[6]. These rotaxanes are able to form one-, two- and three- dimensional polyrotaxane frameworks and thus demonstrating that the structure of the framework can be modified by the metal ion and structure of the pseudorotaxane.²⁷⁻³⁰

The synthesis of one- and two- dimensional polyrotaxanes with CB[6] was accomplished through the use of a 3-pyridyl terminated pseudorotaxanes. The 3-pyridyl diaminobutane containing pseudorotaxane PR43²⁺ (**Figure 13a**) was able to form a 2D coordination polymer network (**Figure 13b**) when reacted with silver nitrate.²⁷ The Ag centre is coordinated to three 3-pyridyl groups from pseudorotaxanes and a nitrate ion to form a distorted tetrahedral geometry. However, when the analogous diaminopentane rotaxane PR53²⁺ (**Figure 13c**) was reacted with silver nitrate, a 1D square-wave shaped polyrotaxane resulted (**Figure 13d**).³¹ In this case, the Ag centre is coordinated to two 3-pyridyl groups and 3 nitrate ions. This topology is due to one of the 3-pyridyl units orienting parallel to the portal opening with a 90° dihedral angle with the six-oxygen plane. As a result, the polymer has a helical structure.

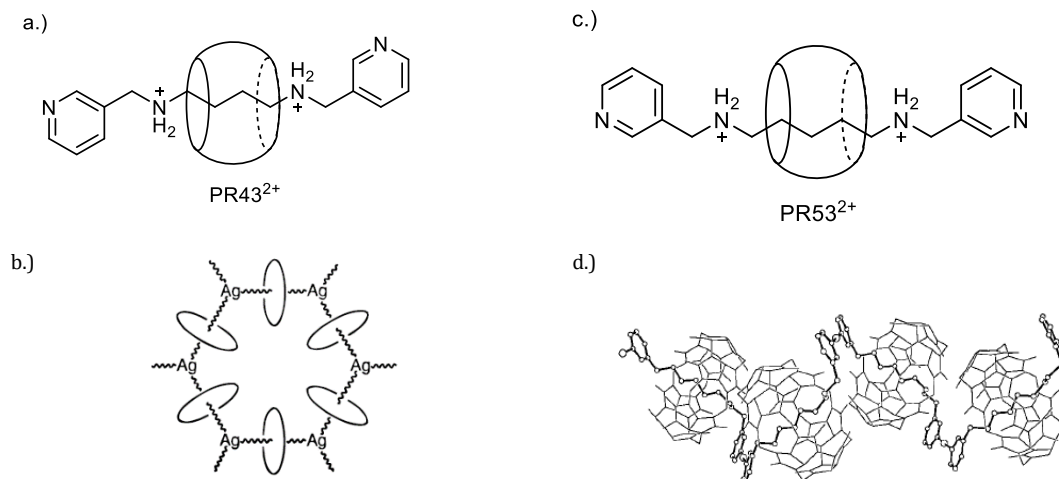


Figure 13. a.) 3-pyridyl diaminobutane pseudorotaxane PR43²⁺ b.) 2d polyrotaxane network formed from reaction of PR4²⁺ and silver nitrate c.) 3-pyridyl diaminopentane pseudorotaxane PR53²⁺ d.) helical 2D polyrotaxane formed from the reaction of PR53²⁺ and silver

Kim and coworkers have also attempted 3D polyrotaxane synthesis using the same synthetic approach. However, all attempts have failed to produce 3D polyrotaxane when using pyridyl terminated pseudorotaxanes and transition metals. Instead, success was found in the use of lanthanide metal ions instead of transition metals because of the larger ionic radii and higher coordination numbers. Furthermore, the use of carboxylate terminated groups would aid the formation of high coordination complexes. 3-phenylcarboxylate diaminobutane pseudorotaxane PCA43²⁺ was able to form a 3D polyrotaxane framework with Tb(NO₃)₃.²⁸

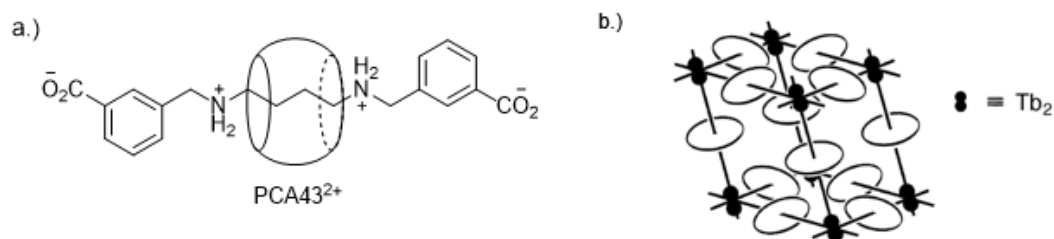


Figure 14. a.) 3-Phenyl carboxylate diaminobutane pseudorotaxane PCA43²⁺ b.) 3D polyrotaxane network formed by reaction with Tb(NO₃)₃. CB is represented schematically with ellipses.²⁸

1.4.4 Dynamics in Metal Organic Rotaxane Framework

The incorporation of mechanically interlocked molecules into a repeating framework of a MORF has potential to produce materials that contain functional entities that may be controlled. These types of mechanically interlocked molecules have previously been studied in solution as molecular shuttles or switches. For the first time, the Loeb research group was able to observe rotational dynamics of the macrocycle of a rotaxanes in the solid state. This MOF was designated **UWDM-1** (University of Windsor Dynamic Material). **Figure 15** shows the tetracarboxylic anilinium rotaxane used to form the MORF with Cu(II) paddlewheels and the MOF formed.¹¹

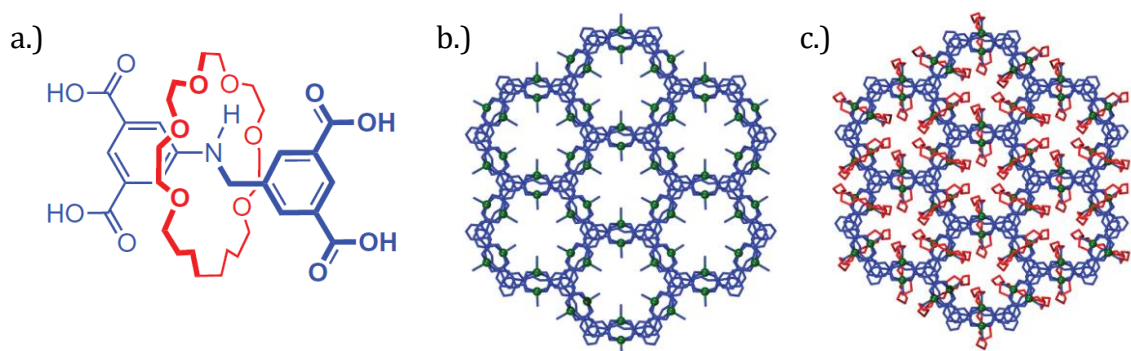


Figure 15. a.) Anilinium rotaxane ligand used in UWDM-1, b.) ball-and-stick representation obtained from single-crystal x-ray diffraction of the polyhedral cavities viewed down c-axis with macrocyclic rings omitted and with macrocyclic rings, b and c, respectively.¹¹

The motions of the macrocyclic wheel were studied through solid-state NMR (SS NMR). The macrocycle was labeled with ^2H (deuterium) through the use of $^2\text{H}_2$ (D_2) during olefin reduction, and was subsequently studied through variable temperature ^2H and ^{13}C SSNMR. The sample was cooled to 160 K and spectral analysis was conducted at increments of approximately 40 K. Comparison of experimental and simulated ^2H SSNMR patterns demonstrated that increased rotational freedom of the macrocyclic wheel was obtained with increased temperature. Modes of motion included a two-site jump of the ^2H , partial rocking and lastly, full rotation of the macrocycle. This was an incredible breakthrough towards the development of molecular machines which had previously only been studied in solution.

The success of this discovery prompted the study of the dynamics of molecular shuttles in MOFs. This was successfully observed again in the Loeb research group, in which the shuttling of a macrocyclic wheel was studied by SSNMR of H-shaped benzimidazolium rotaxanes in the MOF. **Figure 16** depicts the structure of one shuttling unit within the MOF. The tetracarboxylate ligand contains two benzimidazolium recognition sites for the macrocycle to shuttle between. In the MOF, designated **UWDM-4**, the rotaxanes are coordinated to four Zn_4O clusters resulting in a robust dynamic material. ‘Robust dynamics’ describes when the repeated dynamics of one entity, the rotaxane in this case, does not affect the integrity of others linked to it.³²

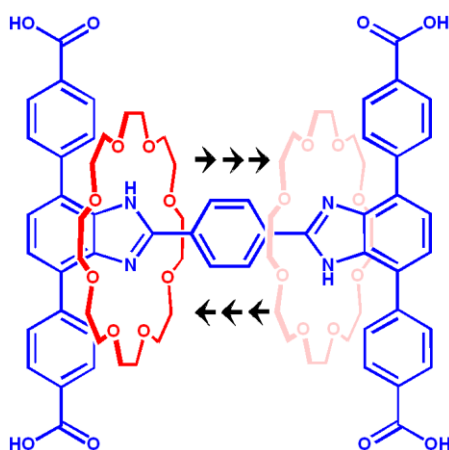


Figure 16. H-Shaped [2]rotaxane shuttle ligand used in MOF UWDM-4.

This discovery has shown that the to and fro motion of MIM switches can successfully function in a highly organized material. This is a critical step towards the creation of solid-state nanodevices from mechanically interlocked molecules if the orientation of the macrocyclic wheel is able to be manipulated and controlled by an external stimulus.

1.5 Scope of Thesis

This thesis involves the synthesis of bis(benzimidazolium) rotaxanes and their incorporation into MOFs. Previously, in the Loeb research group a benzo-bis(imidazolium) rotaxane was able to function as a molecular switch through acid/base chemistry and use of varying macrocycles which showed potential to function as colourimetric and fluorimetric sensors. However, the downfall to these rotaxanes are their insolubility and tendency towards aggregation in solution because of the highly conjugated aromatic system. This, as a result, greatly hinders synthetic endeavours including rotaxane synthesis and MOF synthesis.

In an effort to relieve these problems, the bis(benzimidazolium) rotaxanes were designed. The structural difference between benzo-bis(imidazolium) and bis(benzimidazolium) axles is depicted in **Figure 17**. It was thought that the lack of fused imidazole core and increased flexibility would aid solubility and thus simplify synthetic efforts for both linker and MOF.^{2,33}

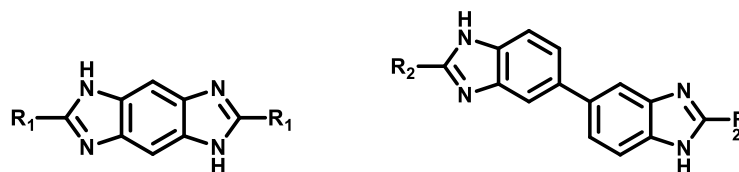


Figure 17. Left: Benzo-bisimidazolium axle core. Right: Bis(benzimidazolium) axle core

This thesis describes the synthesis of [2] and [3]bis(benzimidazolium) rotaxanes and MOF synthesis with these rotaxanes as ligands with Cu(II). **Figure 18** shows the target [2] and [3]rotaxanes with [24]-crown-6 ether wheels. Modification of this design to a non-capped dicarboxylic acid axle allows for the potential synthesis of a CB[7] [2]pseudorotaxane that may also be used as ligand in MOF synthesis.

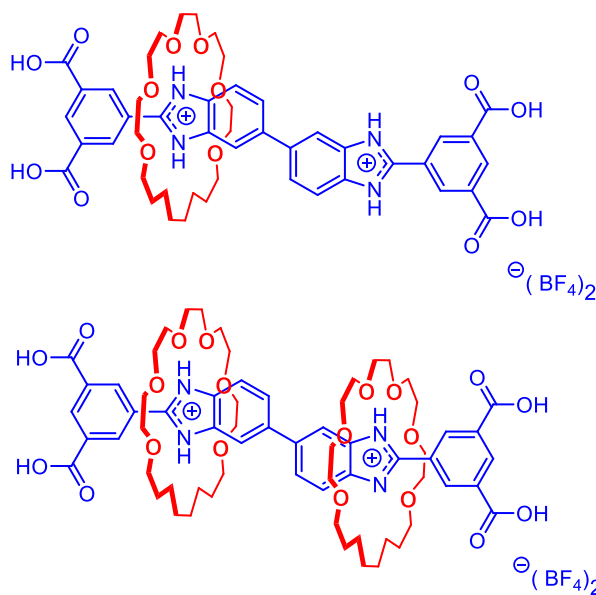


Figure 18. Target [2] and [3]bis(benzimidazolium) rotaxanes

Since the [2]rotaxane contains two recognition sites, it should be able to function as a molecular shuttle and its shuttling rate was studied through VT ^1H NMR. Furthermore, comparisons will be made with their benzo-bis(imidazolium) counterparts that have been previously synthesized to see the effect of the fused recognition sites on shuttling rate in the [2]rotaxane.

Structural comparison with benzo-bis(imidazolium) and a simpler pentaphenyl linker can also be made to speculate on the effect of an extended rotaxane ligand for MOF synthesis. Previously, the benzo-bis(imidazolium) tetracarboxylate ligand had formed non-interpenetrated MOFs with Cu(II) designated University of Windsor Crystalline Material -1 (**UWCM-2**). Similar MOF structures have been reported with more flexible ligands containing isophthalate groups,^{34,35} however, the use of elongated ligands of this type have always resulted in interpenetrated structures.³⁶ Therefore, the lack of interpenetration in UWCM-1 can be attributed to the macrocycle of the rotaxane ligand which occupies the void space.³⁷

Figure 19 depicts the structural differences between previously studied isophthalic terminated ligands. The target [2]rotaxane of this thesis (**Figure 19b**) has an isophthalate C_5 distance of 13.3\AA which is longer than the previously studied benzo-bis(imidazolium) ligand which has a distance of 9.4\AA (**Figure 19a**). Previously, a pentaphenyl tetraacid ligand with isophthalate C_5 distance of 14.4\AA (**Figure 19c**) resulted in formation of an interpenetrated MOF with Cu(II) designated **NOTT-104**. Therefore, the use of this extended rotaxane ligand should result in a non-interpenetrated MOF with larger void space in comparison to the shorter benzo-bis(imidazolium) ligand.³⁶

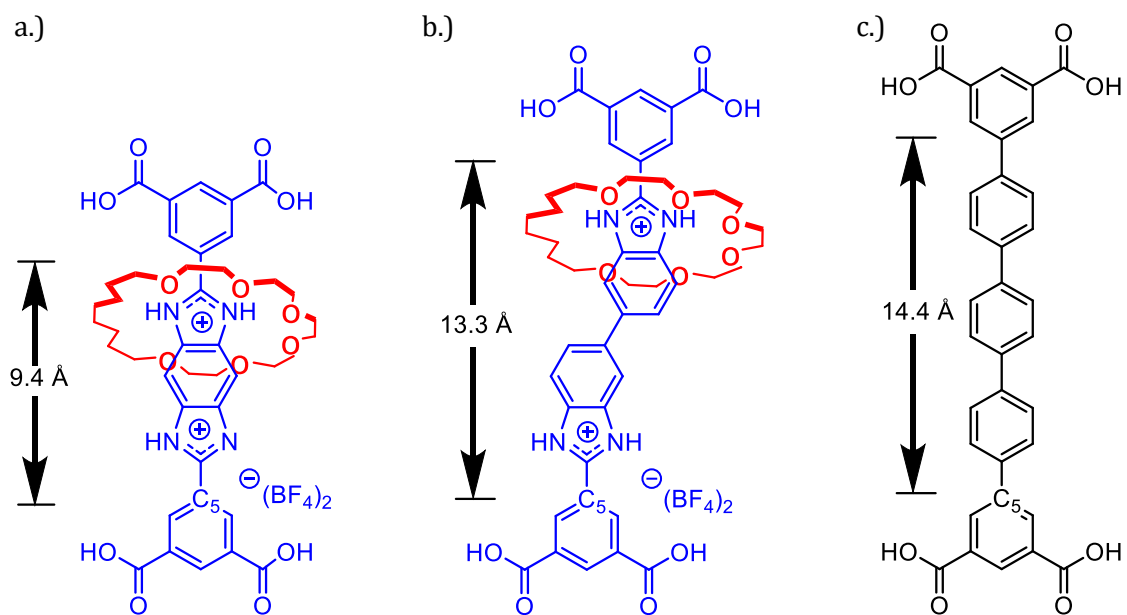
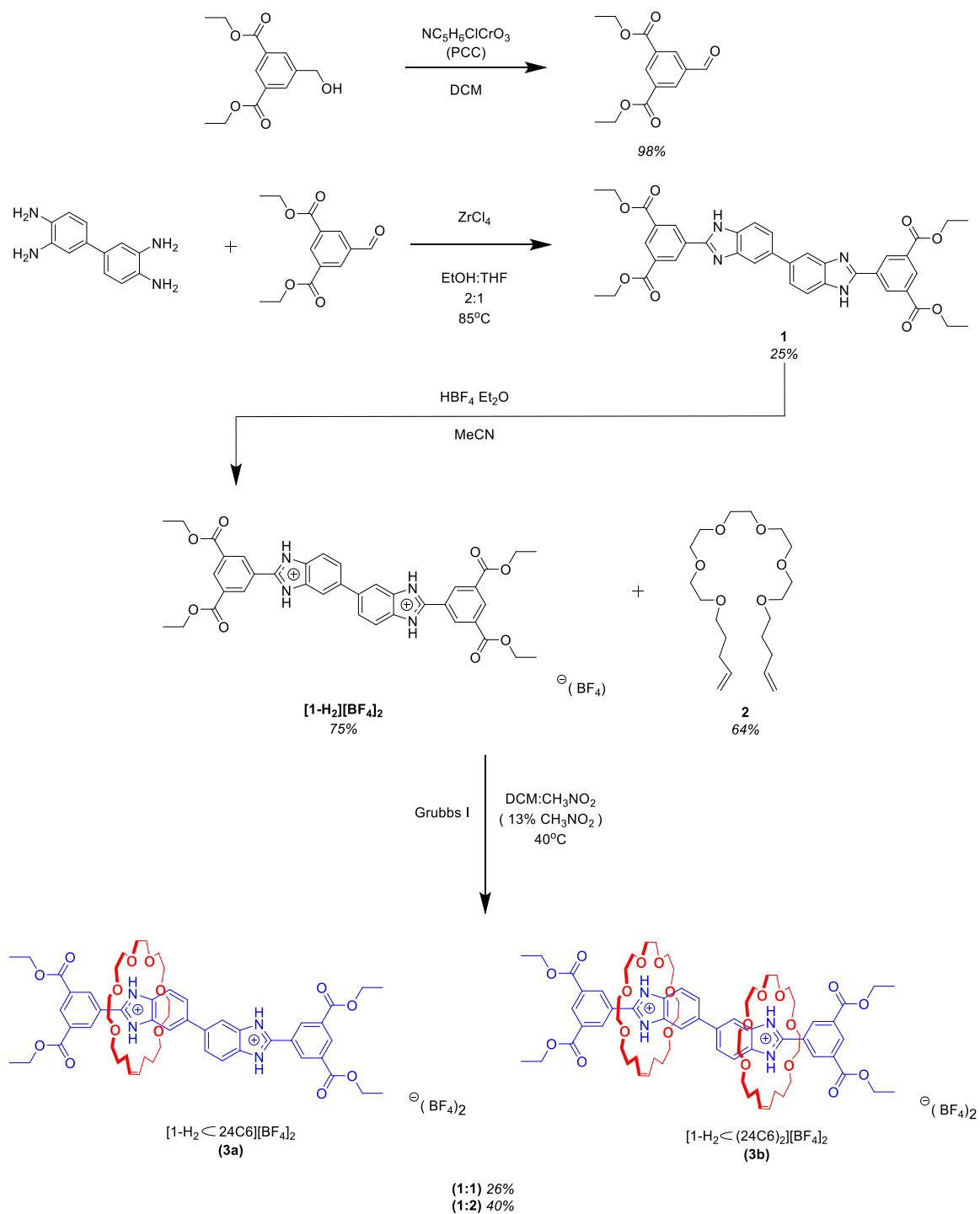


Figure 19. Isophthalate C₅ distance comparison between a.) benzo-bis(imidazolium) [2]rotaxane b.) target bis(benzimidazolium) [2]rotaxane and c.) pentaphenyl tetraacid ligands.

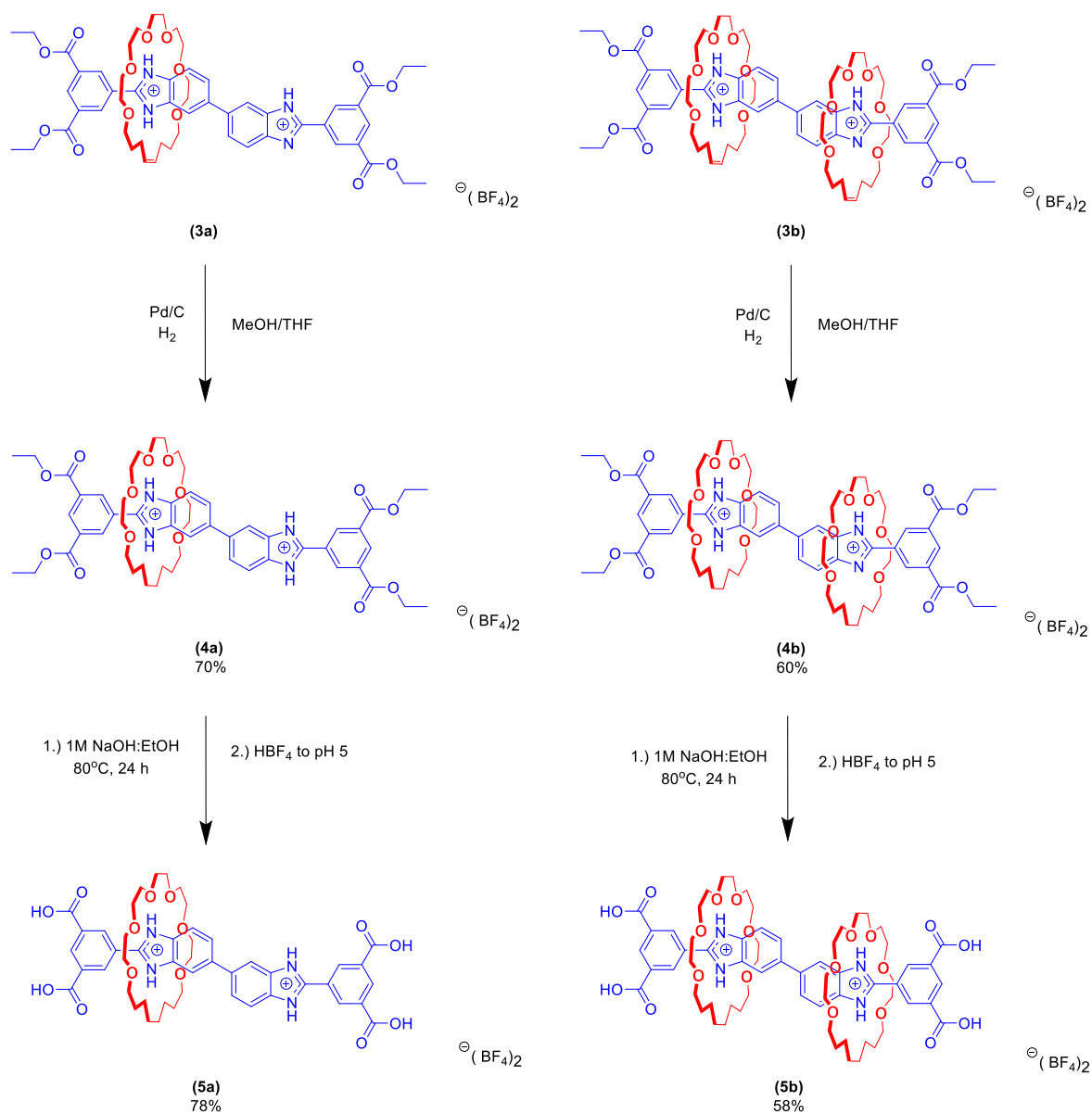
Chapter 2 – Results and Discussion

2.1 Organic Synthesis

Rotaxane synthesis involves a multistep reaction pathway that is seen in Scheme 1 and 2. Axle synthesis first involves the oxidation of diethyl 5-(hydroxymethyl)isophthalate to diethyl 5-formylisophthalate. A condensation reaction was conducted between 3,3'-diamino benzidine and diethyl 5-formylisophthalate using ZrCl_4 to yield the neutral axle (**1**). The axle was then protonated through the addition of $\text{HBF}_4 \cdot \text{Et}_2\text{O}$ to give **[1-H₂][BF₄]₂**. The [24]-crown-6-ether wheel was prepared through tosylation of pentaethylene glycol followed by alkylation with 4-pentene-1-ol to give the 'open' macrocycle or 'pre-crown'. Ring closing metathesis was conducted on the protonated axle and pre-crown using Grubbs I catalyst $\text{RuCl}_2(=\text{CHPh})(\text{PCy}_3)_2$. This yielded a mixture of both [2] and [3]rotaxane. Separation of the mixture was conducted by filtration of crude product in hot EtOAc from which a white solid was obtained and identified as [3]rotaxane (**3b - [1-H₂⊂(24C6)₂][BF₄]₂**). The solvent of the filtrate was removed *via* a rotary evaporator to which Et_2O was added to precipitate a light yellow solid, the [2]rotaxane (**3a - [1-H₂⊂(24C6)][BF₄]₂**). The olefin of the macrocycle was reduced using Pd/C and H_2 to yield **4a** and **4b** and the tetraesters were hydrolyzed using NaOH to yield and reprotonated with HBF_4 to give the final tetraacid rotaxanes (**5a** and **5b**). Details of the synthetic conditions and characterization are found in Chapter 3 - Experimental.



Scheme 1: Reaction scheme for [2] and [3] tetraester rotaxane synthesis



Scheme 2: Reaction scheme for tetraacid rotaxane synthesis

Table 1. Summary of Percent Yield and Total Reaction Efficiency

Axle:Pre-crown	mol% Yield [2]Rotaxane*	mol% Yield [3]Rotaxane*	Total Reaction Efficiency*
1:1	16	9	26%
1:2	23	17	40%

*The % yield of [2] and [3]rotaxane was calculated with respect to moles of axle starting material used.

Comparative reactions of different axle to crown mole ratio were conducted to observe the effect of the amount of macrocycle on [2] and [3]rotaxane preference and overall reaction efficiency, or total rotaxane formation. The total reaction efficiency was found to be 26% and 40% for reactions with 1:1 and 1:2 mole ratio of axle:pre-crown, respectively. The increase in amount of macrocycle increases the total reaction efficiency, however, [2]rotaxane still remains the major product. Reactions with greater than 2 equivalents were also conducted however it was found that the use of excess macrocycle resulted in gradual deprotonation of axle by crown ether. This was observed by the precipitation of white solid within the reaction flask. At this point, the reaction was halted in order to recover the starting material.

The preference for the formation of [2]rotaxane over [3]rotaxane can be attributed to deprotonation of the axle or decrease in binding affinity for the second recognition site once the first macrocycle has associated with the axle. Deprotonation may occur by solvent or crown ether. The crown ether can act as a Lewis base and deprotonate the axle by forming an acid-base complex with BF_4^- . In rotaxane formation, it is pivotal for the presence of a recognition site for template synthesis to be successful. The formation of [3]rotaxane is only possible when both benzimidazole sites are

protonated allowing for both macrocycles to interact with the axle before ring-closing metathesis. However, if gradual deprotonation of bare axle occurs, this eliminates the recognition site for a second macrocycle and thus results in [2]rotaxane as the major product. In addition, the preference may also be due to steric hindrance from the first macrocycle particularly since the wheel is able to shuttle between both sites.

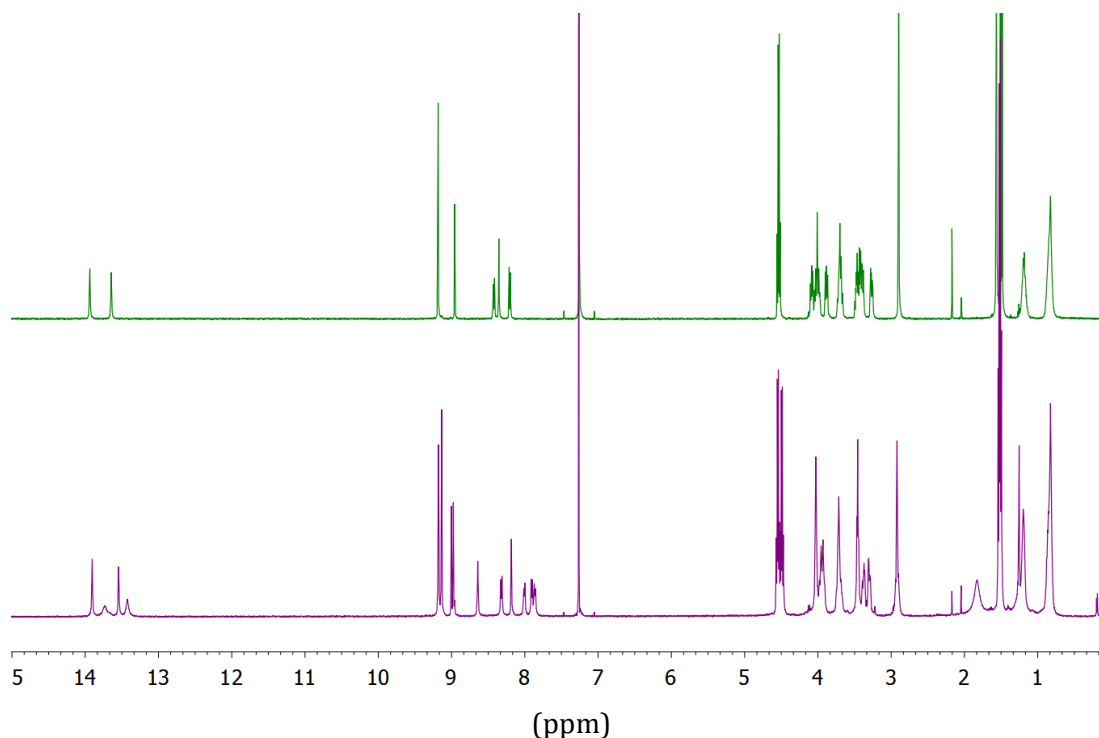


Figure 20. Top: ^1H NMR spectrum of tetraester [3]rotaxane, **4b** and Bottom: ^1H NMR spectrum of tetraester [2]rotaxane, **4a**

Figure 20 depicts the ^1H NMR spectrum of [3]rotaxane (top) and [2]rotaxane (bottom) in CDCl_3 . Since the [2]rotaxane has two recognition sites, it is able to function as a molecular shuttle. In CDCl_3 shuttling was slow on the NMR time scale and peak separation corresponding to complexed and uncomplexed ‘sides’ of the rotaxane are able to be resolved. The most notable differences between the two spectra are the increased number of peaks in the NH (13-14ppm) and aromatic (7.5-9.5ppm) regions.

In the [3]rotaxane, there are two NH peaks at 13.94 and 13.65 ppm corresponding to the *cis* and *trans* conformations of the diprotonated species. The [2]rotaxane shows two sharp NH peaks at 13.91 and 13.54 ppm. These peaks correspond to the NH that are complexed to the macrocyclic wheel. The broader NH peaks at 13.73 and 13.43 ppm correspond to the uncomplexed NH peaks. These peaks are likely broad due to proton exchange with water present in the sample.

Furthermore, the [2]rotaxane shows a more complex aromatic region caused by slow exchange in CDCl₃ which splits the aromatic protons of complexed and uncomplexed sides. Assignment of aromatic [2]rotaxane peaks was determined by 2D ¹H-¹H NMR spectroscopy which shows Nuclear Overhauser Effect (NOE) from nearby nuclei. Initial Nuclear Overhauser Effect Spectroscopy (NOESY) conducted showed low NOE signal information from protons of interest were unable to be obtained. Alternatively, Rotating-frame Overhauser Effect Spectroscopy (ROESY) is able to provide appropriate NOE information for intermediate sized molecules (1000-5000Da) which may show zero NOE signal in a NOESY spectrum. The tetraester [2]rotaxane has a molecular weight of 1101.8 Da and is therefore considered a medium size molecule and appropriate to use for ROESY to determine proton environments as labelled in **Figure 22**.

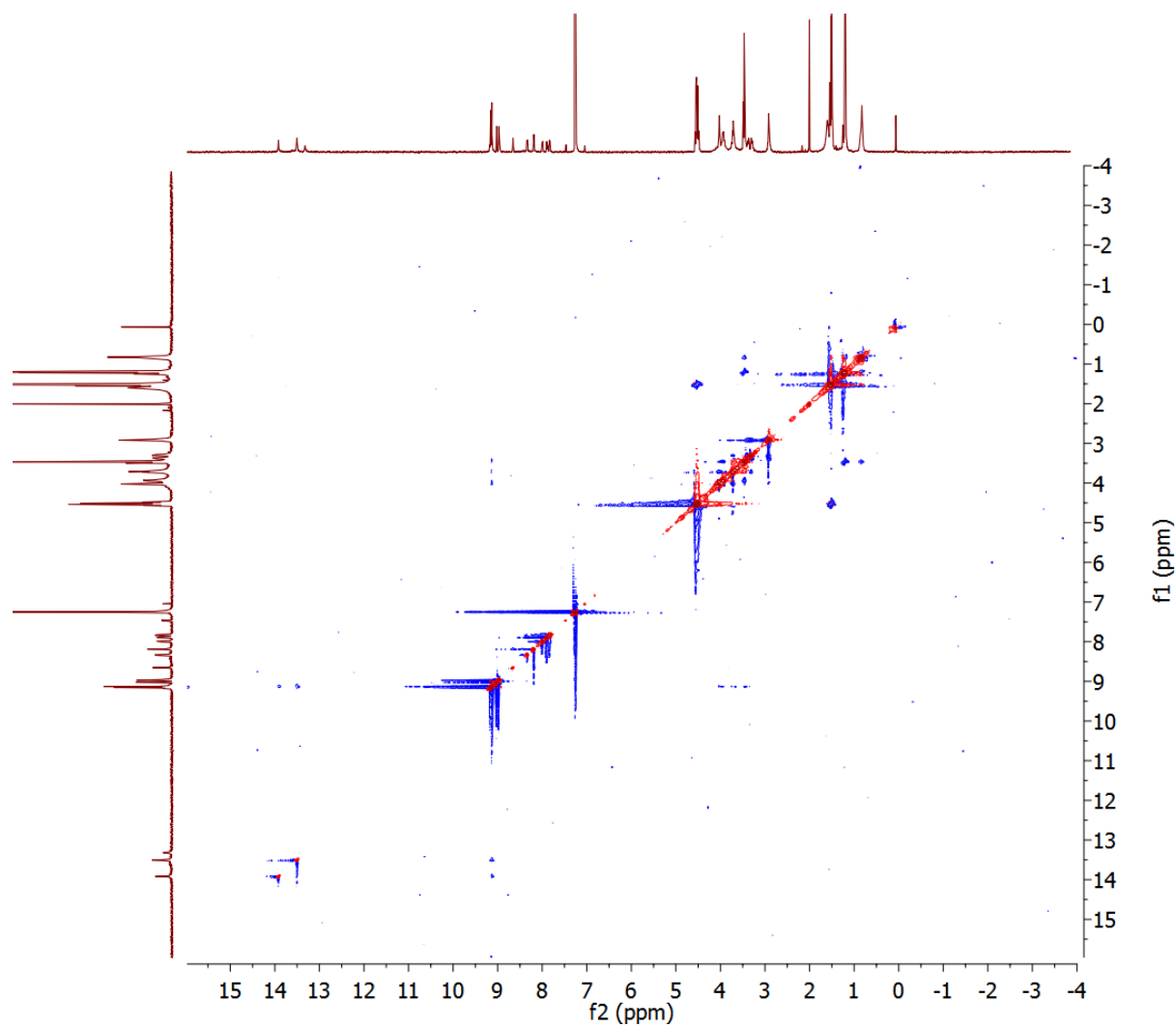


Figure 21. Full ROESY Spectrum of tetraester [2]rotaxane, **4b**. (CDCl_3 at 500 MHz).

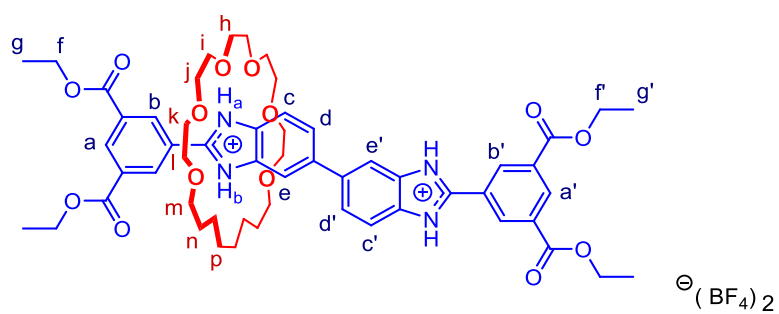


Figure 22. Tetraester [2]rotaxane (**4b**) proton environments.

Shown in **Figure 21** the full ROESY spectrum of **4a**. Proton **b** was able to be assigned because of NOE to NH peaks at 13.91 and 13.54 ppm (**Figure 23**) and NOE to crown ether protons **j**, **h** and **k** (**Figure 24**). Furthermore, the crown ether protons were able to be assigned as observed in **Figure 25**. Cross peaks in the spectrum indicate proton **k** experiences NOE from protons **j** and **l**. As well, proton **i** experiences NOE from protons **j** and **h**. Proton **l** experiences NOE from with proton **m**. Protons **o**, **p** and **n** were assigned as the upfield multiplets with total integration of 12.

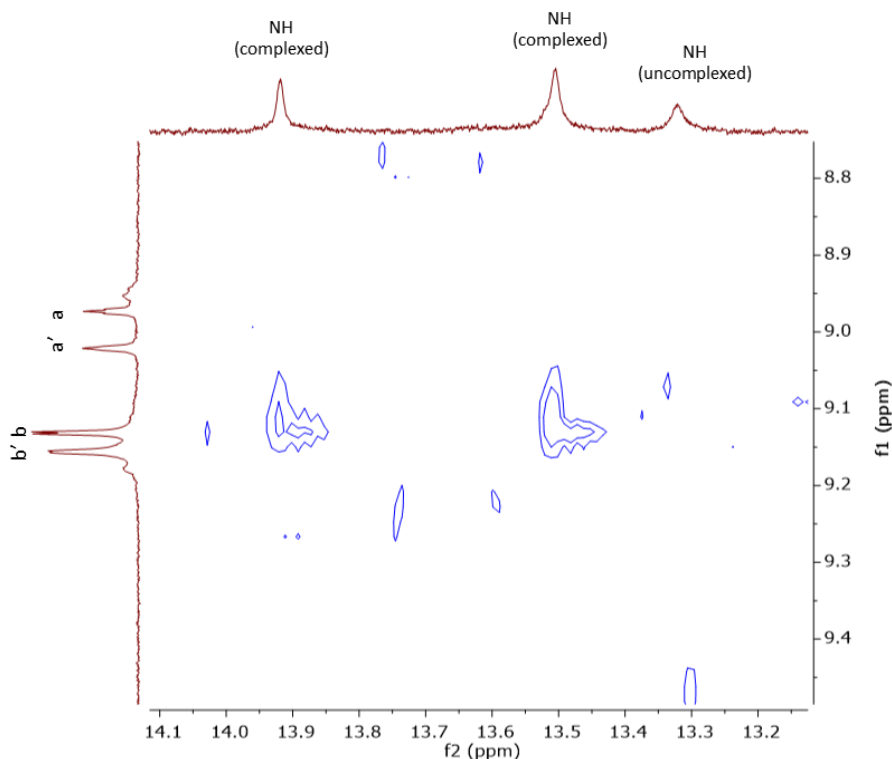


Figure 23. Cross-section of aromatic (*f1*) and NH (*f2*) regions in ROESY of **4b** (CDCl_3 at 500 MHz)

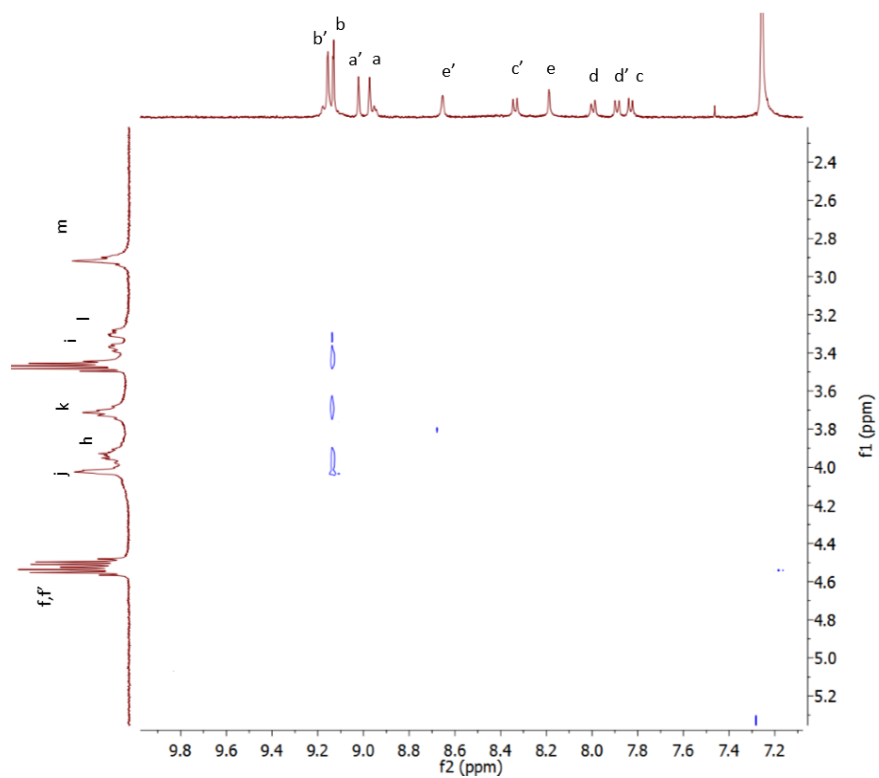


Figure 24. Cross-section of macrocycle (*f1*) and aromatic (*f2*) regions in ROESY of **4b** (CDCl₃ at 500 MHz)

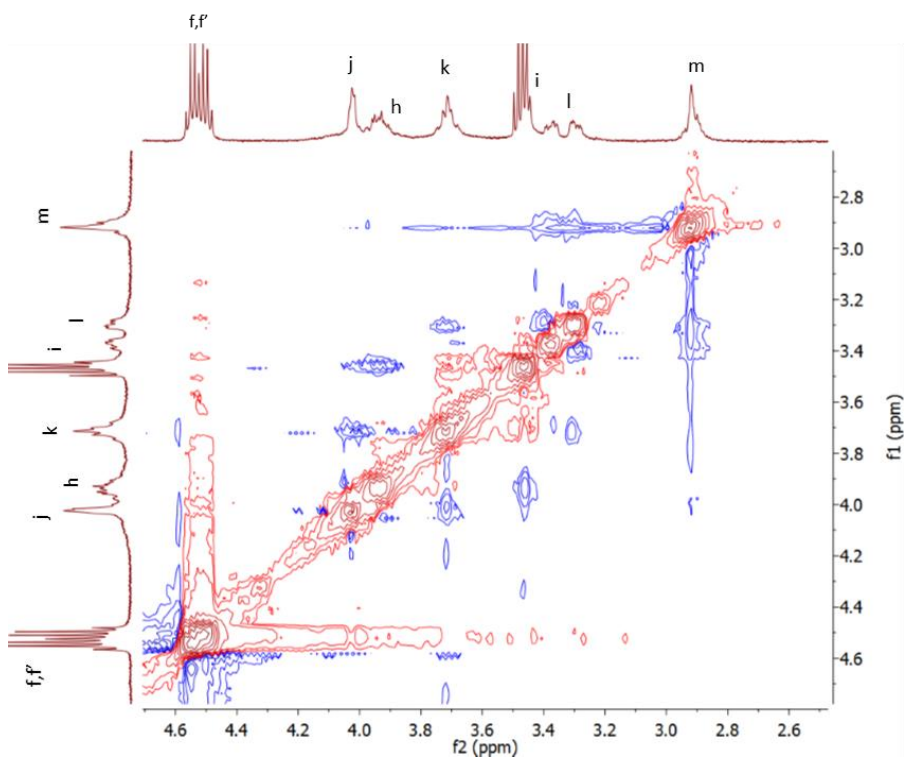


Figure 25. Cross-section of macrocyclic regions (*f1*) and (*f2*) in ROESY of **4b** (CDCl₃ at 500 MHz)

A second ROESY spectrum was obtained in order to assign complexed NH peaks. The majority of the same cross peaks were observed, however, NOE cross peaks were observed with complexed NH peaks and benzimidazole protons **c** and **e**. This allowed the assignment of NH peak at 13.91 to be adjacent to imidazole **e** proton and NH peak at 13.54 to be adjacent to imidazole **c** proton. Furthermore, aromatic protons corresponding to the portion of the axle associated with the complexed crown ether observe fine splitting patterns from coupling to neighbouring protons. Protons on the uncomplexed portion of the axle are not able to show these fine splitting patterns because of proton exchange of uncomplexed NH with water which reduces resolution of the uncomplexed aromatic peaks.

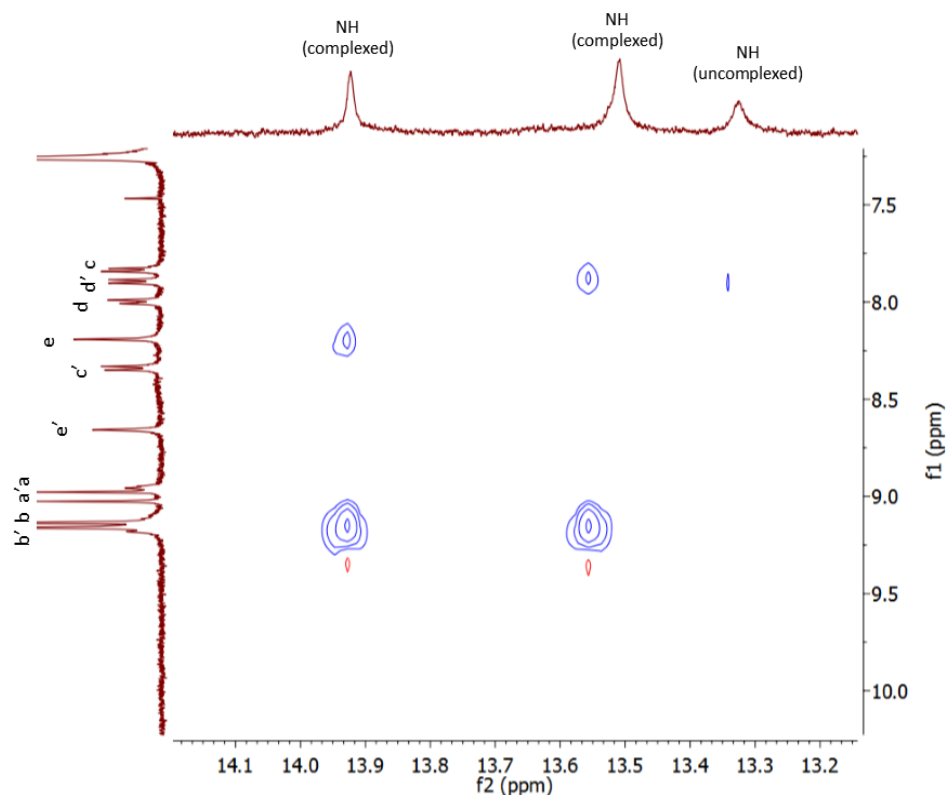


Figure 26. Cross-section of aromatic region (*f1*) and NH region (*f2*) in ROESY of **4b** (CDCl₃ at 500 MHz)

2.2 Determination of Shuttling Rate of [2]Rotaxane

Variable Temperature (VT) ^1H NMR spectroscopy was used to determine the shuttling rate of the [24]-crown-6 macrocycle in the [2]rotaxane, **5a**. First, the choice of solvent was determined by the apparent shuttling rate in various solvents at room temperature. It was found that the [2]rotaxane observes slow shuttling with respect to the NMR time scale in CDCl_3 and CD_2Cl_2 and moderate shuttling in CD_3CN . However, shuttling rates were too slow to determine by 2D Exchange Spectroscopy (EXSY). Therefore, VT ^1H NMR spectroscopy was chosen as the method for shuttling rate determination. The low boiling points of CDCl_3 and CD_2Cl_2 limited the determination of the shuttle rate by (VT) NMR method. Therefore, CD_3CN was used for shuttling studies.

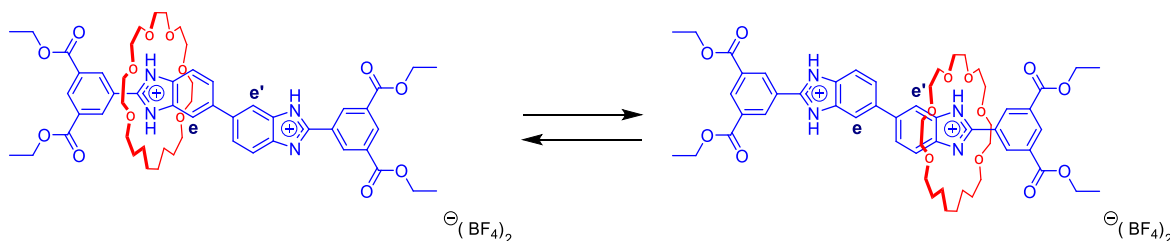


Figure 27. Shuttling states of [2]rotaxane and benzimidazolium proton environment studied via VT ^1H NMR.

Shown in **Figure 27** are the shuttling states and the benzimidazolium protons **e** and **e'** used to probe the shuttling rate of the crown ether. **Figure 28** shows the benzimidazolium N-H and aromatic regions of the VT ^1H NMR spectra. At the lowest temperature, 264 K, two singlets are observed corresponding to protons **e'** (8.32 ppm) and **e** (8.19 ppm) due to the slow shuttling of the macrocyclic wheel. As the sample is warmed incrementally, the two singlets coalesce into one peak at 308 K. After this point, further heating resulted in the development of a sharper singlet that is indicative of fast shuttling.

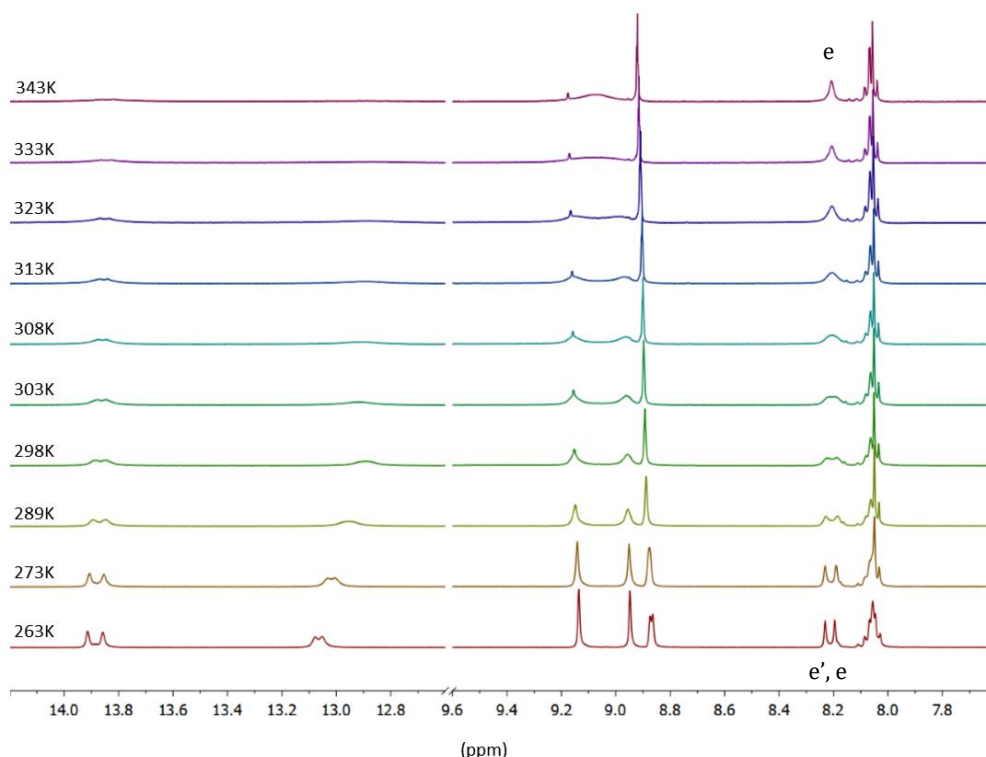


Figure 28. Benzimidazole *N*-H and aromatic regions of variable temperature ^1H NMR of [2]Rotaxane, **5a** (500 MHz in CD_3CN)

In addition to lack of complete coalescence of some peaks, it became evident at higher temperatures that there were trace amounts of impurity present. This impurity is likely to be [3]rotaxane, **4b**. This is further supported by the lack of change in some lower intensity peaks in the aromatic region in each spectrum around 8.05 ppm.

A shuttling rate at each temperature can be determined through line-shape analysis with a simulated spectrum generated through the program dNMR. In order for this method to be accurate, the experimental spectral peaks to be probed must observe Lorentzian line shape. Lorentzian line shape is due to homogenous line broadening and the physical appearance tends towards narrower line wings.

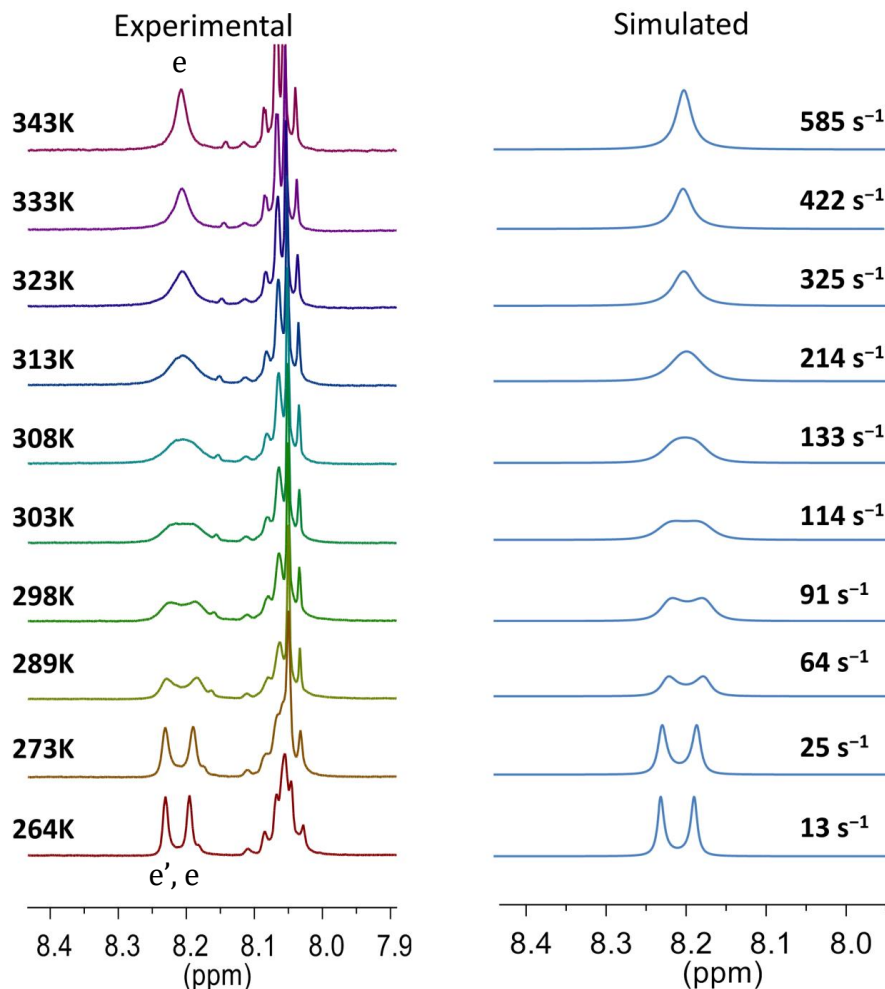


Figure 29. Experimental and Simulated VT ^1H NMR spectrum of **4b**.

Figure 29 shows the experimental and simulated VT ^1H NMR spectrum of **4b** with protons **e** and **e'** labeled. Line-shape analysis with experimental spectra allowed for the estimation of rate constants, k , at each temperature. These k values at their corresponding temperature can be used to construct an Eyring Plot ($1/T$ vs $\ln(k/T)$) to obtain thermodynamic parameters from the equation of the line.

The Eyring Equation $k = \frac{k_B T}{h} e^{\frac{-\Delta G^\ddagger}{RT}}$ relates rate to temperature where k is the rate constant, T is absolute temperature in Kelvin(K), R is the gas constant $1.987 \text{ cal}\cdot\text{K}^{-1}\text{mol}^{-1}$, h is Plank's Constant $1.58 \times 10^{-34} \text{ cal}\cdot\text{s}$, and k_B is Boltzmann's constant $3.30 \times 10^{-16} \text{ cal}\cdot\text{K}^{-1}$.

$^{24} \text{ cal} \cdot \text{K}^{-1}$. Using the relationship of $\Delta G^\ddagger = \Delta H^\ddagger - T\Delta S^\ddagger$, rate can also be expressed in terms of enthalpy, ΔH^\ddagger , and entropy, ΔS^\ddagger as $k = \frac{k_B T}{h} e^{\frac{\Delta S^\ddagger}{R}} e^{\frac{-\Delta H^\ddagger}{RT}}$. The linear form of the Eyring Equation is:

$$\ln \frac{k}{T} = -\frac{\Delta H^\ddagger}{R} \cdot \frac{1}{T} + \ln \frac{k_B}{h} + \frac{\Delta S^\ddagger}{R}$$

Therefore, a plot of $1/T$ vs $\ln(k/T)$ allows for the determination of the thermodynamic parameters of ΔG^\ddagger , ΔH^\ddagger , and ΔS^\ddagger with slope = $-\Delta H^\ddagger/R$ and y-intercept = $\ln k_B/h + \Delta H^\ddagger/R$.

The Eyring plot of shuttling of **4a** is shown in **Figure 30**.

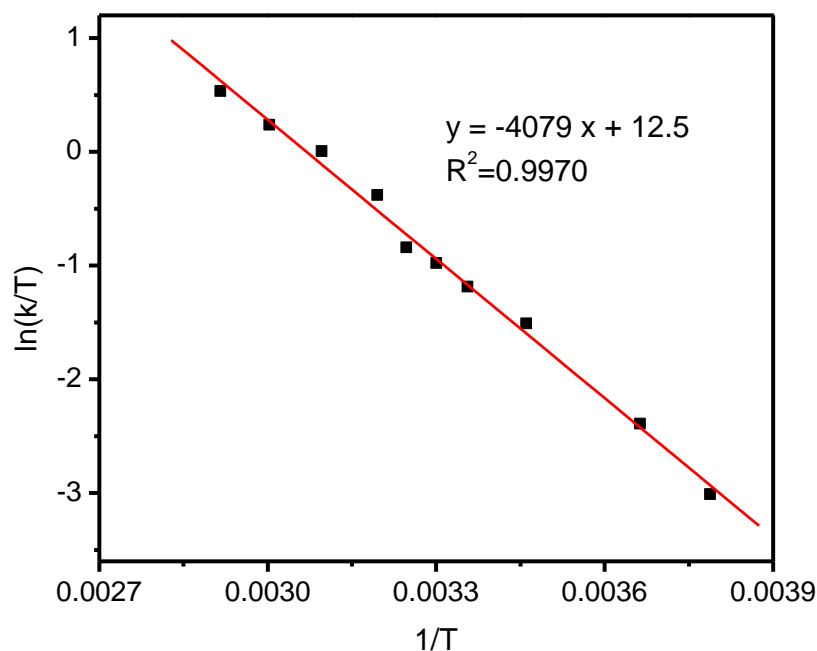


Figure 30. Eyring Plot of shuttling rates of **4b**

From the Eyring plot, it was determined that the shuttling rate, k , at room temperature was 91 s^{-1} . The shuttling energy barrier, $\Delta G^\ddagger_{(298\text{K})}$ was determined to be $14.7 \text{ kcal} \cdot \text{mol}^{-1}$. The thermodynamic parameters ΔH^\ddagger and ΔS^\ddagger were determined to be $8.10 \text{ kcal} \cdot \text{mol}^{-1}$, $\Delta S^\ddagger = -22.3 \text{ cal} \cdot \text{mol}^{-1} \cdot \text{K}^{-1}$.

Table 2. Comparison of Benzo-bis(imidazolium) [2]Rotaxane and Bis(benzimidazolium) [2]Rotaxane Shuttling Rates and Thermodynamic Parameters at 298K.

	Benzo-bis(imidazolium) [2]Rotaxane ³⁷	Bis(benzimidazolium) [2]Rotaxane, 4a
$\Delta G^\ddagger_{(298K)}$ (kcalmol ⁻¹)	13.4	14.7
$\Delta H^\ddagger_{(298K)}$ (kcalmol ⁻¹)	11.2	8.10
$\Delta S^\ddagger_{(298K)}$ (cal•mol ⁻¹ K ⁻¹)	-6.92	-22.3
$k_{(298)}$ s ⁻¹	976	91

The bis(benzimidazolium) rotaxane, **4b**, shows a lower $\Delta H^\ddagger_{(298K)}$ and more negative $\Delta S^\ddagger_{(298K)}$ value than the benzo-bis(imidazolium) rotaxane which uses the same [24]-crown-6 ether wheel. The decreased $\Delta H^\ddagger_{(298K)}$ in the **4b** is attributed to weaker interactions between the crown ether and benzimidazolium core. The non-fused core results in greater electron density around the benzimidazolium NH and therefore causes the NH to be less acid and have weaker hydrogen-bonding interaction with the crown ether oxygen. For both systems, the negative $\Delta S^\ddagger_{(298K)}$ is indicative that some degree of ordering is required for the shuttling to occur. In the case of **4b**, a larger negative ΔS^\ddagger is observed because the flexibility of the non-fused core requires more ordering to enter the transition state. Furthermore, the k at 298K is much slower in **4b** than the analogous benzo-bis(imidazolium) rotaxane. Crown ether shuttling may also be affected by better solvation in CD₃CN of **4b** than the benzo-bis(imidazolium) rotaxane.

2.3 CB[7] [2]Pseudorotaxane

Modification of the bis(benzimidazolium) axle design to a non-capped axle allowed for the study of [2]pseudorotaxane formation with CB[7] in aqueous solution. First, the host-guest complex must be studied in order to determine if the bis(benzimidazolium) core is compatible with the CB[7]. **Figure 31** shows a stack plot comparing spectra of CB[7], 3,3'-diamino benzidine and the inclusion complex formed from 1 equivalent of CB[7] and 1 equivalent of 3,3'-diamino benzidine in 0.1M D₂SO₄ in D₂O.

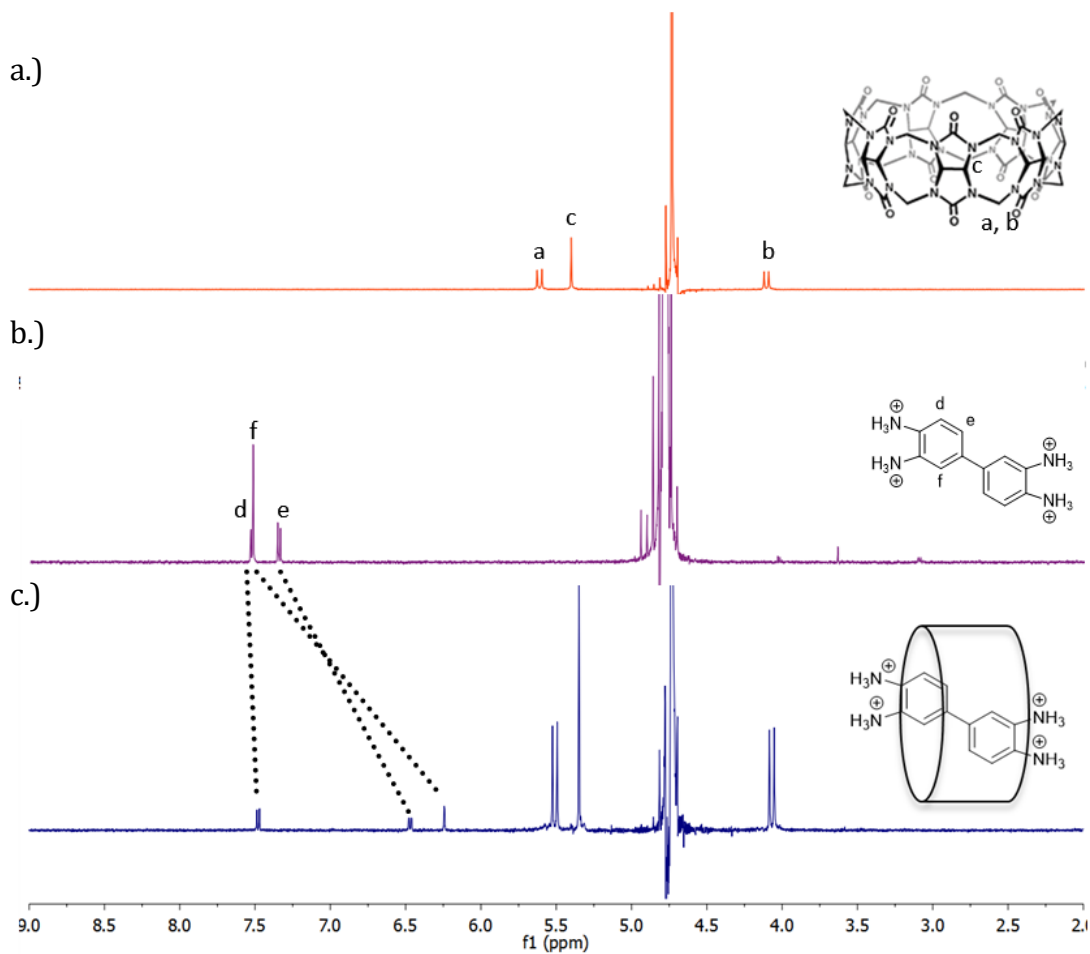


Figure 31. ¹H NMR spectra of a.) CB[7] b.) 3,3'-diamino benzidine c.) inclusion complex of CB[7] and 3,3'-benzidine in 0.1M D₂SO₄ in D₂O at 500 MHz.

In **Figure 32c**, we see there is an upfield shift in all protons associated with the benzidine moiety. This is indicative of the shielding effect caused by the complexation with CB[7]. In addition, there are no peaks corresponding to uncomplexed benzidine or CB[7].

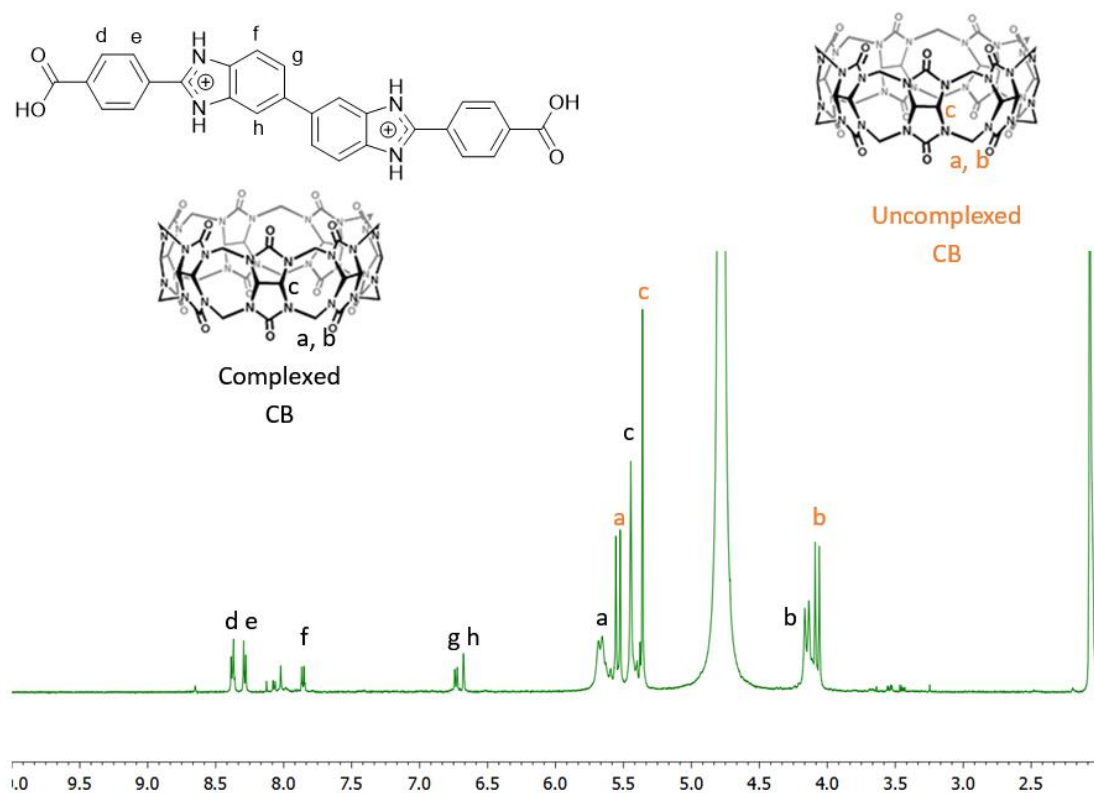


Figure 32. ^1H NMR of [2]pseudorotaxane formation and uncomplexed CB[7] in 0.1M D_2SO_4 in D_2O at 500 MHz.

1 Equivalent of benzoic acid terminated bis(benzimidazolium) axle and 1 equivalent of CB[7] was stirred at 80°C for 16 h in 0.1M D_2SO_4 in D_2O and resulted in the ^1H NMR spectrum in 0.1M D_2SO_4 in D_2O shown in **Figure 32**. These are preliminary results infer the synthesis of a [2]pseudorotaxane. The presence of complexed and uncomplexed CB[7] can be observed as well as unique peaks corresponding to the

complexed axle. The naked axle is insoluble in D₂O, therefore the aromatic peaks observed must correspond to [2]pseudorotaxane. However, attempts to replicate these results were unsuccessful due to impurities found in synthesized axle which ultimately skewed the mole ratio of axle to CB[7]. Impurities could include the 1,4-dibenzoic acid starting material, mono-condensation, and 1,2-substituted product.

Future efforts to obtain pure axle and optimize synthetic conditions for full complexation of CB[7] and axle need to be pursued. Furthermore, potential modification to axle design could afford the interlocked [2]rotaxane which could have potential for MOF incorporation.

2.4 Single-Crystal X-Ray Structures

2.4.1 [2]Rotaxane and [3]Rotaxane

Suitable crystals of tetraester [2]rotaxane (**4a**) or tetraacid [2]rotaxane (**5a**) large enough for single crystal X-ray crystallography were unable to be obtained after many trials. Shown on the left in **Figure 34** are the small needle crystals obtained from slow diffusion of MeOH vapour into a solution of **4a** in DMF. Suitable crystals for single crystal X-ray crystallography of tetraester [3]rotaxane (**4b**) were obtained by slow diffusion of MeOH vapour into a solution of [3]rotaxane in CHCl₃. The right image in **Figure 34** shows the physical appearance of the crystals obtained from slow diffusion of hexane vapour into a solution of **4b** in CHCl₃.

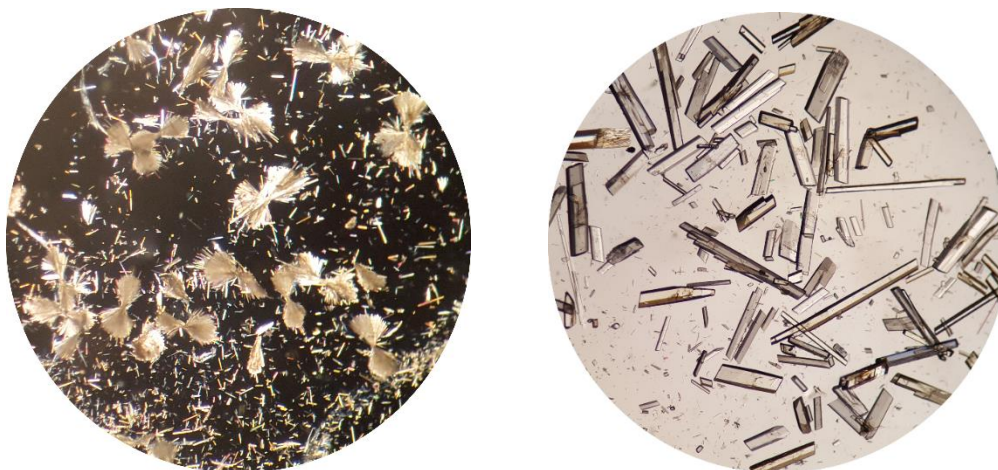


Figure 33. Left: Physical appearance of tetraester [2]rotaxane (**4a**) obtained from slow diffusion of MeOH vapour into a solution of **4a** in DMF. Crystals (small needles of 0.01 mm) are viewed under polarized light for better visualization. Right: physical appearance crystals (blocks of 0.20-0.40mm) of tetraester [3]rotaxane (**4b**) obtained from slow diffusion of hexanes into a solution of **4b** in CHCl₃.

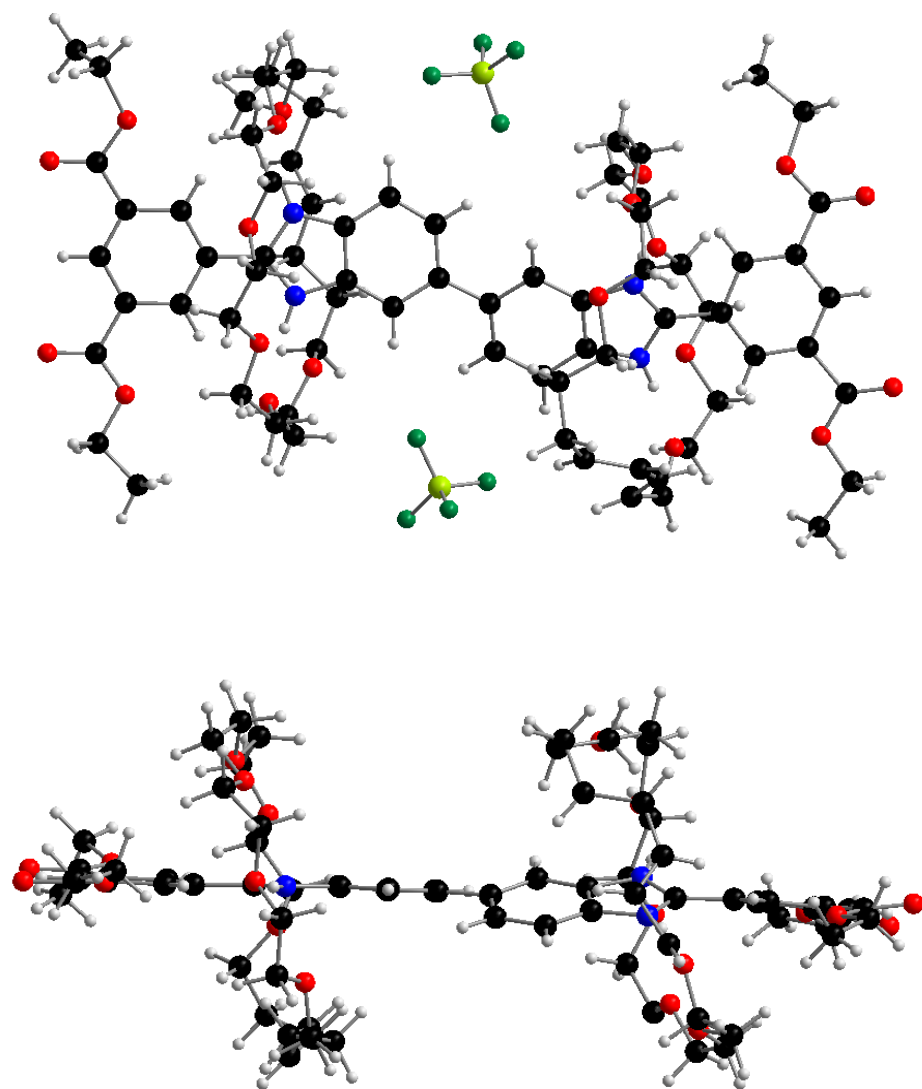


Figure 34. Ball-and-stick representations of X-ray crystal structure of tetraester [3]rotaxane, **4b**. Labeling scheme is black = carbon, blue = nitrogen red = oxygen, green = fluorine, yellow = boron. Left: View perpendicular to axle plane, Right: view along axle plane with counterions omitted for clarity. Solvent molecules omitted for clarity in both representations..

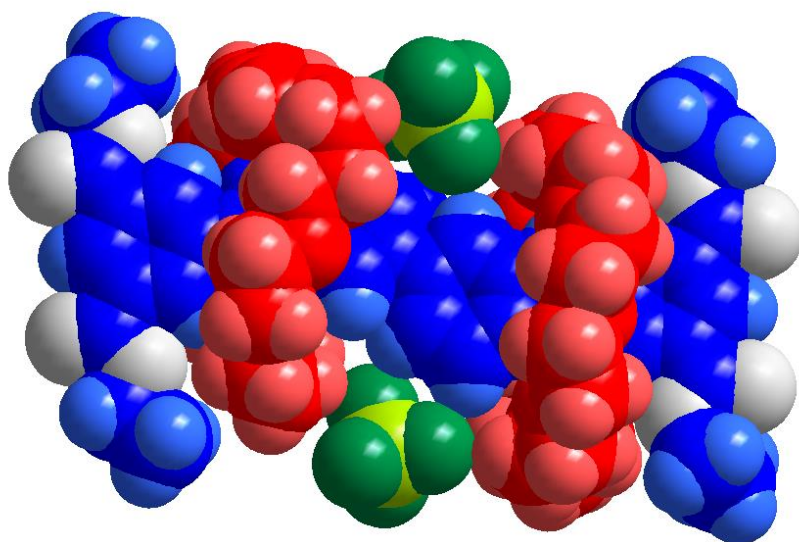


Figure 35. Space-filling diagram of tetraester [3]rotaxane, **4b**. Labeling Scheme is blue = axle, white = axle oxygens, red = wheel, yellow = boron, green = fluorine. Solvent molecules are omitted for clarity.

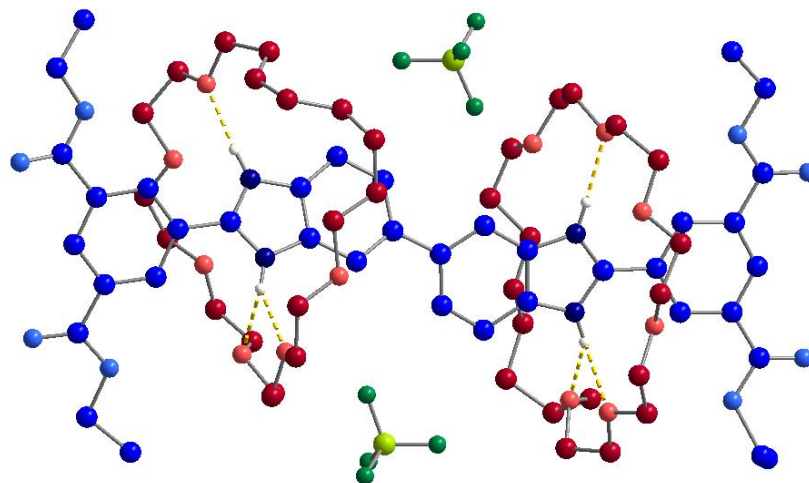


Figure 36. Ball-and-stick representations of X-ray crystal Structure of tetraester [3]rotaxane (**4b**) showing hydrogen bonding interactions between axle imidazole and wheel oxygens shown with yellow dashed line. Protons not involved in hydrogen bonding are removed for clarity. Labeling scheme: blue = axle, red = wheel. yellow = boron, green = fluorine. Solvent molecules are omitted for clarity.

The bis(benzimidazolium) axle is able to adopt *cis*- or *trans*- isomers because of the free rotation about the single bond between the benzimidazole units. Both *cis*- and *trans*- conformations have been observed previously with substituted bis(benzimidazolium) molecules.^{38,39} In **Figure 34**, we see that the bis(benzimidazolium) rotaxane adopts the *trans* conformation. The preference for the *trans* conformation in [3]rotaxane (**4b**) is attributed to the steric bulk imparted by the complexation with the macrocyclic rings. The *trans*- conformation prevents unfavourable electrostatic repulsion between the macrocycles. Furthermore, it should be noted that there is observable torsional angle within the benzimidazole units which indicates that the axle can still have a degree of flexibility even with the presence of two macrocycles. The torsional angle between the two benzimidazole axle planes was measured to be 24.6°.

Figure 37 depicts the π - stacking interaction between layered [3]rotaxane. The π -stacking distance between the centroids of the aromatic rings was calculated to be 3.97 Å. **Figure 38** depicts the space-filling representation of this packing. Here we are able to see the alternating arrangement of the macrocycles while still allowing close enough interaction for π -stacking.

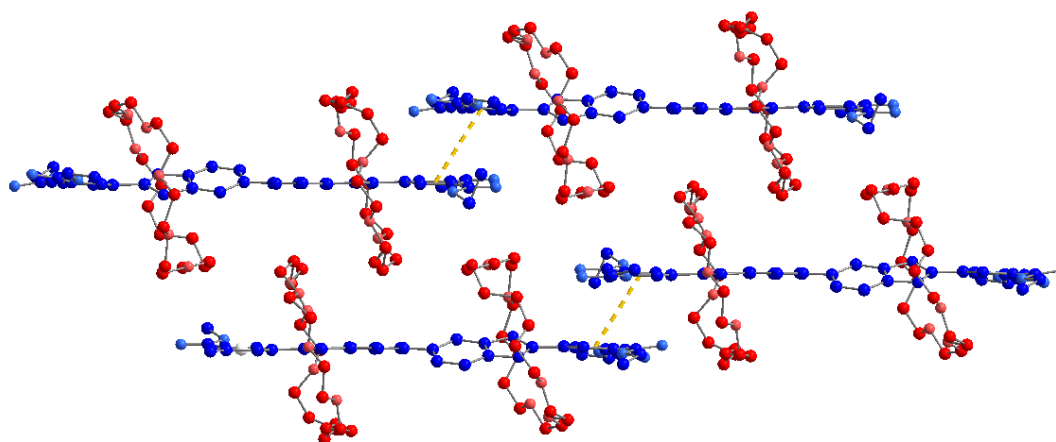


Figure 37. Ball-and-stick representation of π -stacking interactions between [3]rotaxane with π -stacking distance represented by yellow dashed line. Hydrogen atoms, counter ions and solvent molecules omitted for clarity. Labelling scheme: axle = blue, wheel = red.

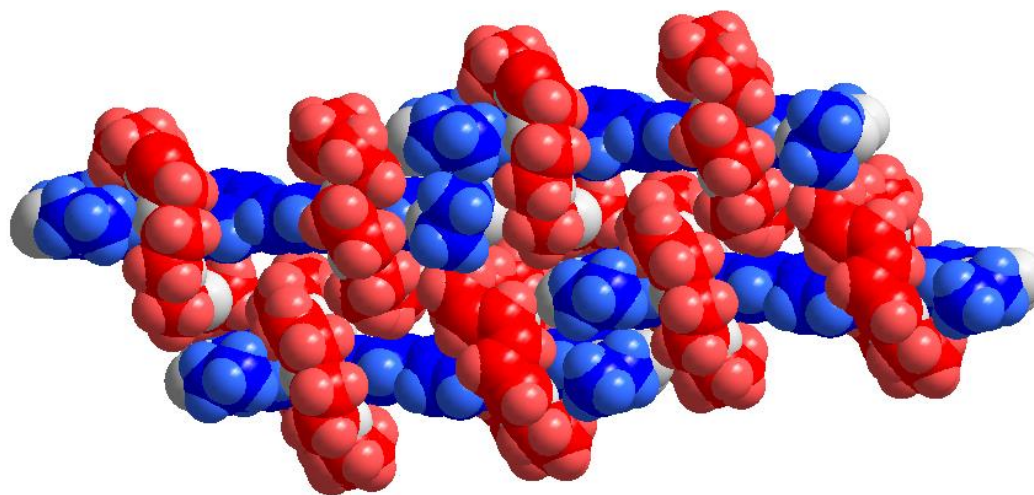


Figure 38. Space-filling representation of [3]rotaxane packing. Labelling scheme: axle = blue, wheel = red, oxygen = white. Counter ions and solvent molecules omitted for clarity.

A further look into the packing arrangement of the rotaxane we see that the BF_4^- anion and CHCl_3 solvent molecules (for which the crystals were obtained from) form a layer between hydrogen bonding stacks of rotaxane, **Figure 39** and **Figure 40**.

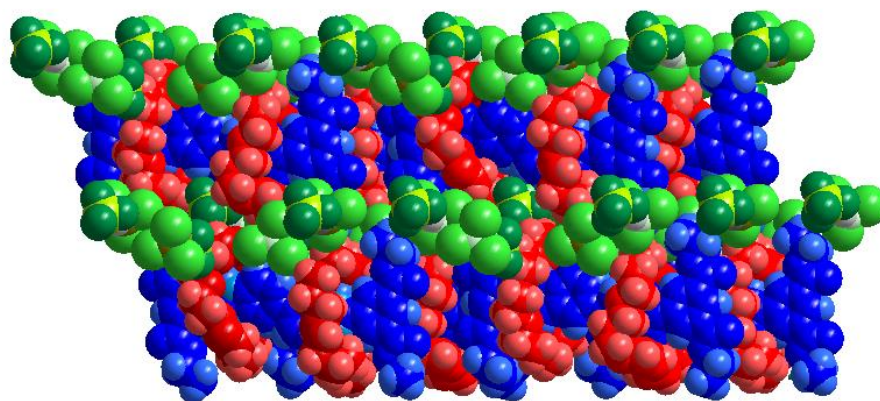


Figure 39. Space-filling representation of packing of [3]rotaxane between solvent and counterion layer. Labelling Scheme: Blue = axle, red = wheel, dark green = fluorine, yellow = boron, light green = CHCl_3 carbon, neon green = chlorine.

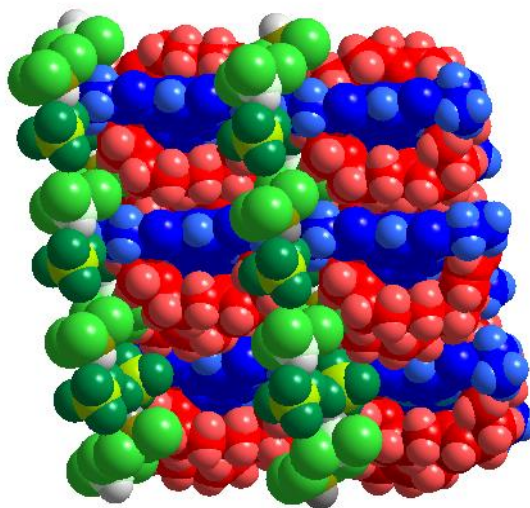


Figure 40. Space-filling representation of [3]rotaxane packing between solvent and counterion layer along c-axis. Labelling scheme: Blue = axle, red = wheel, dark green = fluorine, yellow = boron, light green = CHCl_3 carbon, neon green = chlorine.

We again see the alternating arrangement of the macrocycles in the packing of the rotaxanes. The CHCl₃ and BF₄⁻ anion are hydrogen bonded and form the separating layer between the stacks.

Table 3. Crystal Data and Solution Results for Tetraester [3]Rotaxane, **4b**.

Crystal Data	
Molecular Formula	C ₇₆ H ₁₀₆ B ₂ Cl ₆ F ₈ N ₄ O ₈
Formal Weight (g/mol)	1590.01
Crystal System	triclinic
Space Group	<i>P</i> -1
<i>a</i> (Å)	15.910(6)
<i>b</i> (Å)	17.404(3)
<i>c</i> (Å)	18.462(4)
α (°)	96.880(2)
β (°)	111.096(2)
γ (°)	110.378(2)
<i>Z</i>	4
ρ , g cm ⁻³	1.324
μ , mm ⁻¹	2.41
Solution Results	
reflections used	40810
variables	1028
restraints	7
<i>R</i> ₁ [<i>I</i> > 2σ (<i>I</i>)] ^[a]	0.1411
<i>R</i> ₁ (all data)	0.1734
<i>R</i> _{2w} [<i>I</i> > 2σ (<i>I</i>)] ^[b]	0.4626
<i>R</i> _{2w} (all data)	0.4138
GoF on <i>F</i> ²	1.7240

^[a] $R_1 = \sum ||F_o| - |F_c|| / \sum |F_o|$; ^[b] $R_{2w} = [\sum [w(F_o^2 - F_c^2)^2] / \sum [w(F_o^2)^2]]^{1/2}$, ^[b] where $w = q[\sigma^2(F_o^2) + (aP)^2 + bP]^{-1}$

2.4.2 MOF Synthesis

Solvothermal synthesis is a widely used method for obtaining crystalline MOF material. This process involves the gradient heating and cooling of a reaction mixture in a sealed vessel. Furthermore, this method utilizes slow conversion from an acidic environment to a basic environment due to the gradual decomposition of DMF (or DEF) to dimethylamine (or diethylamine) during the heating process. This allows for gradual deprotonation of the carboxylic acid groups of the rotaxane ligand and allows for coordination with metal ions. This process is also driven by the self-assembly of the metal atoms and ligands to form MOF.⁴⁰

A solvent system of DEF/EtOH/H₂O was initially tested. This system has been shown successful for the previously studied benzo-bis(imidazolium) rotaxane and it served as an excellent starting point for trials.³⁷ A programmable oven was used in order to control heating and cooling times. Warm up and cool down rates were both set at 1°C min⁻¹. [2] and [3]rotaxane MOFs were prepared in similar manners using Cu(NO₃)₂•2.5 H₂O. Table 4 and 5 outline the MOF conditions used for each trial.

For each trial, the 1 equivalent of ligand and 2 equivalents of Cu(NO₃)₂•2.5 H₂O were weighed out separately into vials using an analytical balance. The ligand was dissolved in DMF (or DEF) and the Cu(NO₃)₂•2.5 H₂O was dissolved in EtOH and H₂O. The Cu(NO₃)₂ solution was then transferred to the ligand solution to which a few drops of concentrated HNO₃ acid were added. This mixture was transferred to a borosilicate screw cap vial and heated in a programmable oven.

Table 4. MOF Synthesis Trials with Tetraacid [2]Rotaxane (**5a**)

Trial	Solvent System	Solvothermal Conditions	Result
1	2:1:1 DEF:EtOH:H ₂ O 1.5 mL:0.75 mL:0.75 mL 3 drops of Nitric Acid	Warm up to 85°C over 1 h Constant Heating for 24 h Cool to RT (23.5°C) over 10 h	Mixture of aggregate and cubic crystals
2	4:1:1 DEF:EtOH:H ₂ O 2.0 mL:0.5 mL:0.5 mL 3 drops of Nitric Acid	Warm up to 85°C over 1 h Constant Heating for 24 h Cool to RT(23.5°C) over 10 h	Cubic crystals of varying size
3	2:1:1 DMF:EtOH:H ₂ O 1.5 mL:0.75 mL:0.75 mL 3 drops of Nitric Acid	Warm up to 85°C over 1 h Constant Heating for 24 h Cool to RT (23.5°C) over 10 h	Crystalline aggregates

Table 5. MOF Synthesis Trials with Tetraacid [3]Rotaxane (**5b**)

Trial	Solvent System	Solvothermal Conditions	Result
1	2:1:1 DEF:EtOH:H ₂ O 1.5 mL:0.75 mL:0.7 mL 3 drops of Nitric Acid	Warm up to 85°C over 1 h Constant Heating for 24 h Cool to RT (23.5°C) over 10 h	Aggregates and precipitation of uncomplexed ligand
2	1:1:1 DEF:EtOH:H ₂ O 1.5 mL:0.75 mL:0.75 mL 1 drop of Nitric Acid	Warm up to 85°C over 1 h Constant Heating for 24 h Cool to RT (23.5°C) over 10 h	Aggregates and precipitation of uncomplexed ligand
3	1:1:1 DMF:EtOH:H ₂ O 1.5 mL:0.75 mL:0.75 mL 1 drop of Nitric Acid	Warm up to 85°C over 1 h Constant Heating for 24 h Cool to RT (23.5°C) over 10 h	Aggregates and little precipitation of uncomplexed ligand
4	1.5:1.5:0.1 DMF:EtOH:H ₂ O 1.5 mL:1.5 mL:0.1 mL 1 drop of Nitric Acid	Warm up to 85°C over 1 h Constant Heating for 24 h Cool to RT (23.5°C) over 10 h	Blue/green powder
5	1:1:0.5 DMF:1,4-Dioxane:H ₂ O 1.0mL:1.0mL:0.5mL 1 drop of Nitric Acid	Warm up to 85°C over 1 h Constant Heating for 24 h Cool to RT (23.5°C) over 10 h	Aggregate of crystal plates

The solvent system for MOF trials was modified after the crystal growth period and examination of the physical crystal structure under microscope. Timing of crystal formation (*i.e.* during heating or cooling phase) was also monitored during process.

[2]Rotaxane MOF growth was observed early during the heating phase in Trial 1. This is indicative of crystal growth occurring too quickly and resulted in the formation of some crystal aggregates which were unsuitable for single crystal X-ray diffraction. This prompted later trials with increased amount of DEF in order to increase the solubility of ligand and slow crystal growth and allow for the formation of larger crystals. An additional trial was attempted with DMF instead of DEF but resulted in only crystalline aggregates.

[3]Rotaxane MOF growth Trial 1 resulted in very few crystal aggregates and mostly precipitation of uncomplexed ligand. Furthermore, the crystal aggregates formed during the cooling phase, which indicates that crystal growth was too slow. Trial 2 was attempted with less nitric acid added. The decrease in amount of acid would increase the speed of crystal formation because less acid was needed to be neutralized by the base (diethyl amine). The crystal aggregates in Trial 2 formed during the heating phase, however there was still precipitation of uncomplexed ligand. This is indicative of poor ligand solubility and prompted the change of organic solvent from DEF to DMF in Trial 3. In Trial 3, less ligand precipitation was observed but still resulted in crystal aggregates formation. A decrease in H₂O was employed in Trial 4 to increase ligand solubility and slow crystal growth; the result was blue-green powder during the

heating phase and no crystalline material. Finally, during Trial 4, Ethanol was replaced with 1,4-dioxane and aggregates of crystal plates were obtained.

2.4.3 [2]Rotaxane and [3]Rotaxane MOFs

Figure 41 shows the physical appearance of the crystals obtained from the Trials 1 and 2 of MOF synthesis using [2]rotaxane, **5a**, as ligand. Reaction of tetraacid [2]rotaxane (**5a**) with $\text{Cu}(\text{NO}_3)_2 \cdot 2.5\text{H}_2\text{O}$ through solvothermal synthesis with a solvent system of 2:1:1 DEF:EtOH:H₂O resulted in the formation of a mixture of cubic crystals and crystal aggregates as seen in **Figure 41a**. A solvent system of 4:1:1 DEF:EtOH:H₂O resulted in the formation of cubic shaped crystals that have a layered appearance seen in **Figure 41b**. This was a more successful trial because of the increased homogeneity of crystal appearance and lack of crystal aggregates seen in Trial 1. However, the layering of crystal growth resulted in poor single crystal X-ray diffraction.

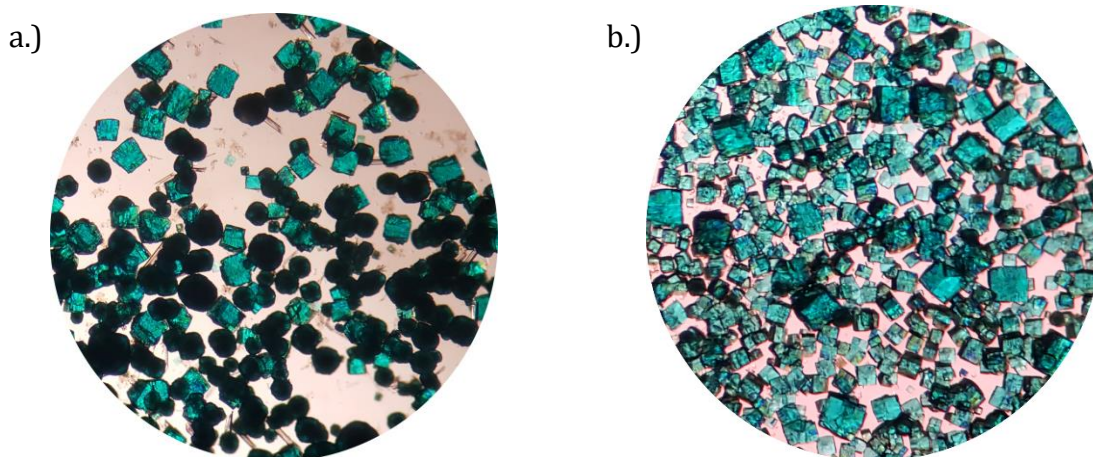


Figure 41. [2]Rotaxane MOF crystals obtained from the reaction of tetraacid[2]rotaxane, **5a** with $\text{Cu}(\text{NO}_3)_2 \cdot 2.5\text{H}_2\text{O}$ through solvothermal synthesis with a.) a solvent system of 2:1:1 DEF:EtOH:H₂O in Trial 1 b.) a solvent system of 4:1:1 DEF:EtOH:H₂O in Trial 2.

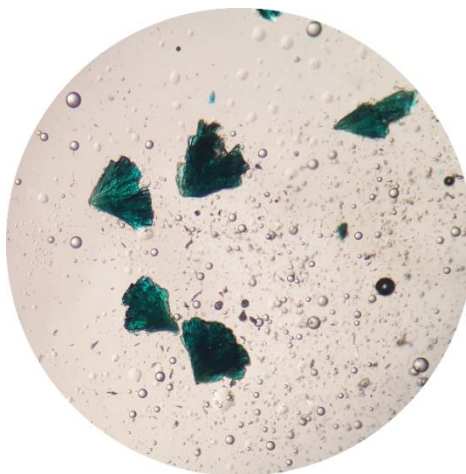


Figure 42. [3]Rotaxane MOF crystals obtained from reaction of tetraacid [3]rotaxane, **5b**, with $\text{Cu}(\text{NO}_3)_2 \cdot 2.5\text{H}_2\text{O}$ through solvothermal synthesis with a solvent system of 1:1:0.5 DMF:1,4-Dioxane: H_2O

Reaction of tetraacid [3]rotaxane (**5b**) with $\text{Cu}(\text{NO}_3)_2 \cdot 2.5\text{H}_2\text{O}$ through solvothermal synthesis with a solvent system of 1:1:0.5 DMF:1,4-Dioxane: H_2O resulted in aggregates of crystal plates. Shown in **Figure 42** are fragments from a larger aggregate in paraffin oil. Again, due to the poor quality of crystals and twin growth, sufficient X-ray diffraction was not able to be obtained. Both [2]rotaxane MOF and the previously studied benzo-bis(imidazolium) MOF (UWCM-2) obtained similar looking cubic crystals seen in **Figure 43**. This may be an indicator that a similar high symmetry MOF was obtained.



Figure 43. The physical appearance of cubic crystals obtained the reaction of tetraacid benzo-bis(imidazolium) [2]rotaxane and $\text{Cu}(\text{II})$ metal.

2.5 Powder X-Ray Diffraction

Since suitable single crystals for X-ray diffraction could not be obtained, powder X-ray diffraction is able to give insight into the structure of the crystalline materials. **Figure 44** shows a comparison of the PXRD patterns of Trial 1, which contained aggregate and cubic crystals and Trial 2, which contained more homogeneous cubic crystals throughout. Trial 1 shows a mixture of peaks corresponding to the different crystalline materials. However, Trial 2 results in a cleaner PXRD pattern with only peaks corresponding to the cubic crystals, with the low 2θ peak at 2.6° matching the peak in Trial 1.

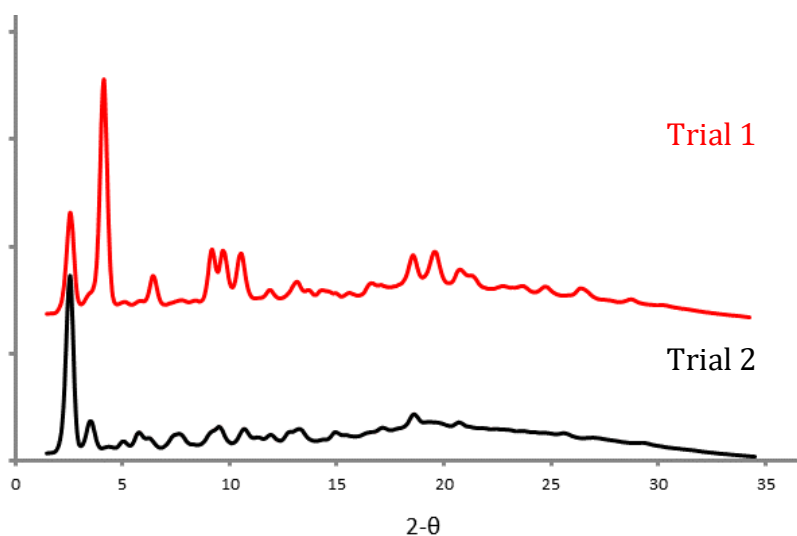


Figure 44. PXRD pattern of [2]rotaxane **5a** MOF synthesis Trial 1 (red) and Trial 2 (black). Trial 1 resulted in the formation of a mixture of aggregate and cubic crystals meanwhile Trial 2 resulted in the formation of uniform cubic crystals.

Figure 45 shows a comparison of experimental PXRD patterns of UWCM-2, [2]rotaxane MOF, [3]rotaxane MOF and simulated PXRD pattern of NOTT-104. Similar to the benzo-bis(imidazolium) MOF, [2]rotaxane MOF has a low 2θ peak which indicates that the crystalline material might be isorecticular (having the same

connections and lattice) to the benzo-bis(imidazolium) MOF. The low 2θ peak at 2.6° corresponds to a d spacing of 34.0 \AA and thus potentially has larger cavities than benzo-bis(imidazolium) rotaxane, which has a 2θ peak of 2.9° corresponding to a d spacing of 30.3 \AA . This finding is consistent with the longer length of the axle which has a C_5 isophthalate distance of 13.3 \AA in comparison to the benzo-bis(imidazolium) rotaxane with a distance of 9.4 \AA . Furthermore, the lack of higher 2θ peaks suggests a lack of interpenetration. In contrast, the crystalline material obtained from [3]rotaxane **5b** results in a distinct PXRD pattern which contains higher 2θ peaks at 4.8° and 10.8° .

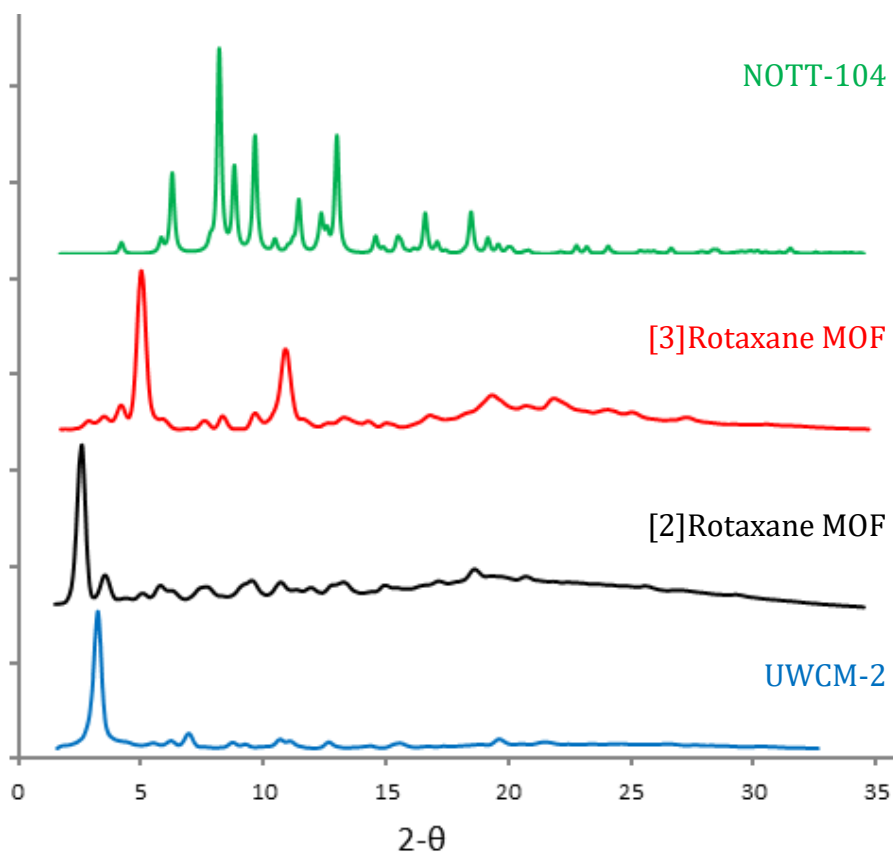


Figure 45. Experimental PXRD patterns of UWCM-2 (blue), [2]rotaxane MOF (black), [3]rotaxane MOF (red) and simulated PXRD pattern of NOTT-104 (green).

Although detailed structural information cannot be confirmed without single-crystal X-ray diffraction, the PXRD pattern of [2]rotaxane MOF shows some evidence

of a potentially similar MOF structure when using benzo-bis(imidazolium) rotaxane as ligand (UWCM-2). **Figure 46** shows a ball-and-stick representation of the framework within UWCM-2. The rotaxanes coordinate to dimeric Cu(II) paddlewheels which self-assemble into cubooctahedral cages (nanoballs).

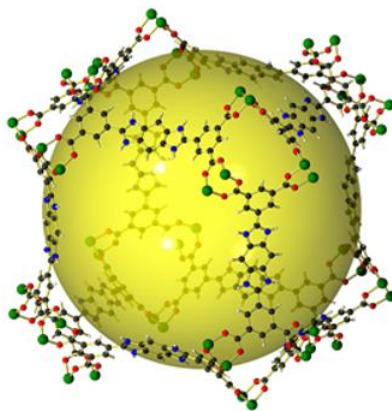


Figure 46. Ball-and-stick representation of the cubic cavity within the framework. Macrocycles are omitted for clarity. The rotaxanes coordinate to dimeric Cu^{II} paddlewheels which self-assemble into cubooctahedral cages (nanoballs). The yellow sphere represents the solvent accessible space within the MOF.³⁷

NOTT-104 uses an analogous pentaphenyl isophthalic ligand and results only in an interpenetrated MOF. The simulated PXRD pattern of NOTT-104 shows higher 2θ peaks corresponding to the different spacing within the interpenetrated networks. These distinctive higher 2θ peaks are not observed in the PXRD patterns of [2] or [3]rotaxane MOF. Since the axle used for [2] and [3]rotaxane ligands are similar in length as the pentaphenyl ligand, this result might be an indicator that the presence of the macrocyclic wheel(s) decreases interpenetration within the MOF. This can be attributed to the bulky macrocycles that occupy the void space that would otherwise be filled by an interpenetrated network.

2.6 Summary and Future Work

Bis(benzimidazolium) [2] and [3]rotaxanes were successfully synthesized and characterized. The packing structure of tetraester [3]rotaxane was characterized and revealed the preference for the trans- conformer. Through axle modification, preliminary results of the formation of a CB[7] [2]pseudorotaxane have been obtained. Further efforts to optimize synthetic conditions for full complexation of CB[7] and axle should be further investigated. The [2]pseudorotaxane also has potential to act as a ligand for MOF synthesis because of the terminal carboxylate groups. Further modification to ligand design through the use of different terminating groups would allow the formation of MOFs with unique topologies. For example, capping of the [2]pseudorotaxane to form the interlocked [2]rotaxane would be an additional aspect that could be studied.

Two distinct crystalline materials were obtained from MOF synthetic attempts when using [2] and [3]rotaxanes **5a** and **5b** as ligands and reacted with Cu(II). The material obtained from [2]rotaxane may have structural similarities with UWCM-2 because of the similar low 2θ angle and lack of higher 2θ peaks. The material obtained from [3]rotaxane **5a** is crystalline and results in a distinct PXRD but further studies need to be conducted to confirm the MOF structure.

Future work includes the optimization of MOF solvothermal conditions in order to obtain single crystals suitable for X-ray diffraction. This would allow determination of the MOF topology and show how the addition of a second macrocyclic ring affects the MOF structure. Furthermore, the use of a rotaxane rather than an extended aromatic system has been previously shown to increase rigidity in MOF structure and

prevent interpenetration. The increase in cavity space could introduce potential to study the translational motion of the macrocycle in the solid-state of this extended [2]rotaxane ligand.

Chapter 3 - Experimental

3.1 General Comments

Diethyl 5-formylisophthalate, 3,3'-diamino benzidine tetramine, pentaethylene glycol, Grubbs I catalyst and 1,4-benzoic acid were purchased from Sigma Aldrich and used as received. Deuterated solvents were obtained from Sigma Aldrich or Cambridge Chemicals and used as received. Thin layer chromatography was performed using Teledyne Silica gel 60 F₂₅₄ plates and viewed under UV light. Column chromatography was conducted using Silicycle Ultra Pure Silica Gel (230 – 400 mesh). ¹H NMR and ¹³C NMR spectra were performed on a Brüker Advance 500 instrument, with a frequency of 500.13 MHz for ¹H nuclei and 125.7 MHz for ¹³C nuclei. Chemical shifts are reported in ppm relative to tetramethylsilane, using the residual solvent peak as a reference standard. All single crystal X-ray data were collected on a Brüker APEX diffractometer with a CCD detector operated at 50 kV and 30 mA with MoK α radiation. Powder XRD measurements were recorded on a Brüker D8 Discover diffractometer equipped with a GADDS 2D-detector and operated at 40 kV and 40 mA.

3.2 Synthesis of **1** and $[1-H_2][BF_4]_2$

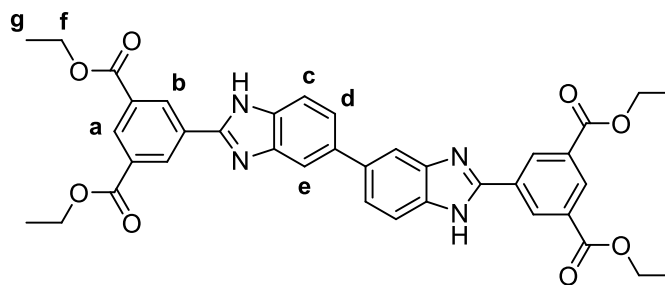


Figure 47. Chemical structure and proton environments of **1**

3,3'-diamino benzidinetetramine (0.428 g, 2 mmol) and a catalytic amount of $ZrCl_4$ (0.093 g, 0.4 mmol) were added to a 2:1 mixture of degassed EtOH:THF under N_2 atmosphere. Diethyl 5-formylisophthalate⁴¹ (1.0 g, 2.0 mmol) was added and the temperature was increased to 85 °C and the mixture was allowed to reflux for 48 h after which the nitrogen flow was stopped and the reaction allowed to reflux in air for 24 h. The solution was allowed to cool to room temperature before placing on ice for 30 min. This resulted in the precipitation of a yellow solid which was filtered off by vacuum filtration. Isolated yield of **1** (0.407 g, 23%). M.P. 180 °C

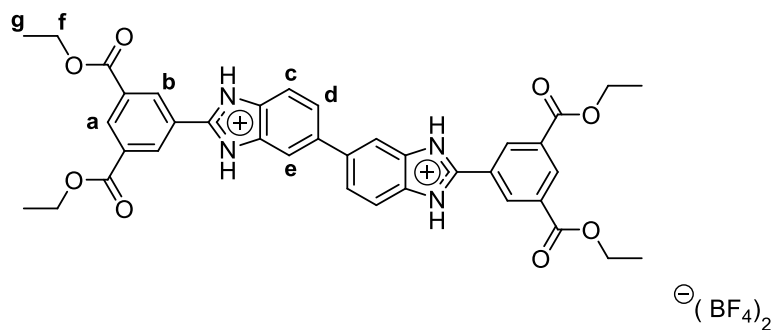


Figure 48. Structure and proton environments of $[1-H_2][BF_4]_2$

1 (0.664 g, 1 mmol) was suspended in MeCN (50 mL) and 5 equivalents of $HBF_4 \cdot Et_2O$ (0.796, 5 mmol) were added dropwise and allowed to stir for 1 h. Solvent was removed *via* a rotary evaporator; the residue was washed twice with Et_2O (20 mL)

to remove excess acid and then filtered to give a white solid (0.691g, 87%) . M.P. > 275 °C (Dec.)

¹H NMR (500 MHz, DMSO): δ = 11.21 **NH** (s(broad) 2H), 10.58 **NH** (s(broad), 2H), 8.96 **b** (d, 4H, ⁴J = 2.5 Hz), 8.55 **a** (d, 2H, ⁴J = 2.5Hz), 7.89 **e** (s, 2H), 7.78 **c** (d, 2H, ³J = 13.5Hz), 4.45 **f** (q, 8H, ³J = 11.5 Hz), 1.41 **g** (t, 14H, ³J = 11.5Hz)

¹³C NMR (126 MHz, DMSO): δ = 164.7, 149.2, 137.2, 135.9, 132.0, 131.9, 131.8, 128.7, 128.7, 124.74, 115.7, 113.2, 62.2, 14.7.

3.3 Synthesis of 2, Pentaethyleneglycol-dipent-4-enyl ether

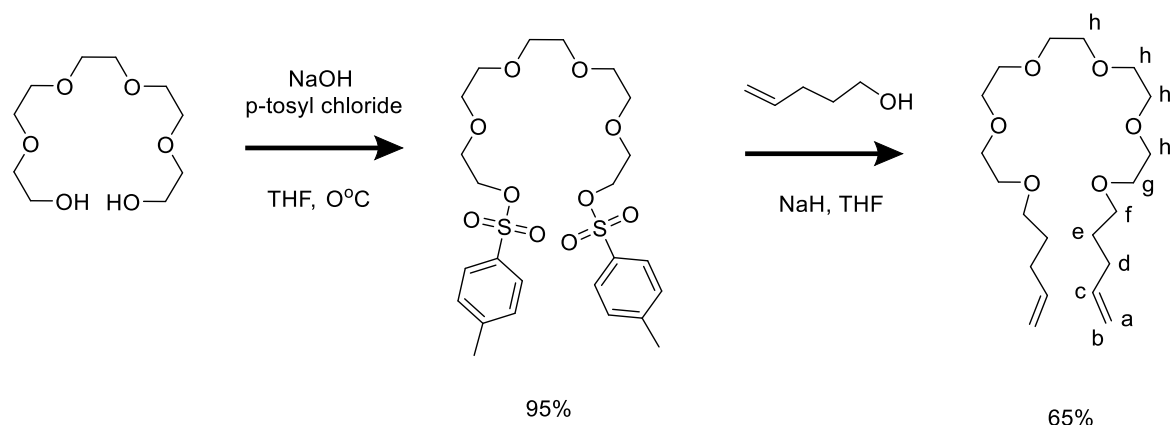


Figure 49. Synthetic pathway, structure and proton environments of Pentaethyleneglycol-dipent-4-enyl ether.

Ditosylated pentaethylene glycol was prepared according to literature procedure.⁴² NaH in 60% mineral oil (15.7 g, 0.393 mol) was slowly added to 200 mL of dry THF under nitrogen at 0°C. 4-pentene-1-ol (33.8 g, 0.393 mol) was dissolved in 40 mL of THF and added to the reaction mixture dropwise and allowed to stir for 1 h. 1,14-Ditosyl-3,6,9,12-tetraoxatetradecane (21.45 g, 0.039 mol) was dissolved in 125 mL of THF and added slowly to the reaction mixture *via* a syringe. The reaction mixture was allowed to warm up to room temperature and stirred for 48 h after which the reaction was quenched with 500 mL of water. The non-aqueous solvent was removed *via* a rotary evaporator and a two layer extraction was performed using CHCl₃ (3 x 250 mL). The aqueous phase was discarded and the organic layer was washed with 1 M HCl (2 x 100 mL), dried over MgSO₄, and the solvent removed to yield a light yellow oil. The product was purified by column chromatography (3:2 v/v, EtOAc/Hexanes) R_f = 0.4, to yield a colourless oil; isolated yield (6.45 g, 43%), M.P: 115°C.

^1H NMR (500 MHz, CDCl_3): δ = 5.81 **c** (m(broad), 2H), 5.02 **b** (m 2H), 4.96 **a** (m, 2H), 3.65 **h** (s, 16H), 3.56 **g** (m(broad), 4H), 3.46 **f** (t, 4H), 2.11 **d** (m(broad), 4H), 1.68 **e** (m(broad), 4H).

^{13}C NMR Data (126 MHz, CDCl_3): δ = 139.02, 114.88, 71.07, 70.65, 30.81, 29.46.

3.4 Synthesis of **3a** and **3b**

[**1-H₂**][BF₄]₂ (0.30 g, 0.35 mmol) was added to a 100 mL Schlenk flask. Pentaethyleneglycol-dipent-4-enyl ether (0.13 g, 0.35 mmol) was added directly to the Schlenk flask. The flask was purged and backfilled with N₂. 7.5 mL of nitromethane was added to the Schlenk and allowed to stir until all components were in solution. 50 mL of DCM was added to the stirring solution under N₂. Grubbs I catalyst, [RuCl₂(=CHPh)(PCy₃)₂] (29 mg, 10 mol%) was dissolved in 1 mL of dichloromethane and added to the stirring solution under N₂. The reaction was refluxed at 40°C for 18h after which 5% catalyst was added to the reaction and allowed to reflux for 24 h. 5 mol% was added at 24 h intervals until a total of 25 mol% catalyst. Reaction progress was monitored by ¹H NMR. Solvent was removed *via* a rotary evaporator and the crude product was sonicated in hexanes to yield a grey-green solid. This solid was suspended in acetonitrile to which HBF₄ Et₂O (0.15 g, 0.94 mmol) was added dropwise and allowed to stir for 1 h. Solvent was removed with a rotary evaporator and the residue was sonicated in diethyl ether to remove excess acid. Diethyl ether was decanted and dichloromethane was added to the solution; the solution was allowed to sit for 1 h to allow unreacted axle to precipitate out. The mixture was then filtered through Celite and the solvent was removed *via* rotary evaporator. Hot ethylacetate was used to filter off white solid (44 mg, 0.03 mmol) of E- and Z- isomers of [3]rotaxane, **3b**. M.P > 300°C (Dec.). The filtrate solvent was removed by rotary evaporate and the residue was filtered with Et₂O to give light green solid (69 mg, 0.05 mmol) of E- and Z- isomers [2]rotaxane, **3a**. M.P > 300°C (Dec.).

3a, [1-H₂C24C6][BF₄]₂

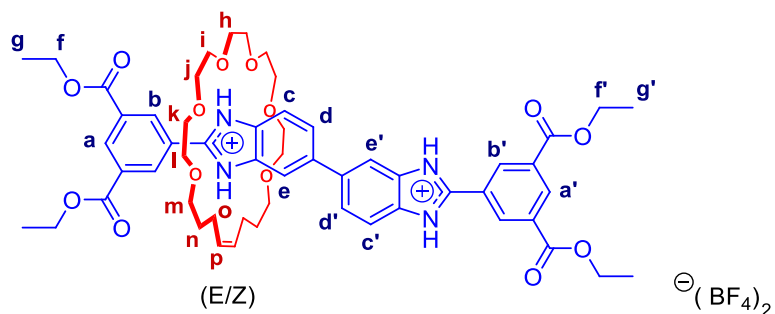


Figure 50. Structure and proton environments of **3a**

¹H NMR (500 MHz, CDCl₃): δ = 14.05 NH (s, 2H), 13.66 NH (s, 2H), 9.16 **b** (s, 2H), 9.11 **b'** (s, 2H), 9.01 **a'** (s, 2H), 8.96 **a** (s, 2H), 8.66 **e'** (s, 2H), 8.33 **c'** (d, 2H), 8.17 **e** (s, 2H), 8.00 **d** (d, 2H), 7.89 **d'** (d, 2H), 7.82 **c** (d, 2H), 5.08 **p** (s, 2H), 4.69 **p'** (s, 2H), 4.52 **f, f'** (m, 8H), 4.09 **j** (m, 4H), 3.93 **h** (m, 4H), 3.72 **k** (m, 4H), 3.38 **i** (m, 4H), 3.34 **l** (m, 4H), 2.91 **m** (m, 4H), 1.74 **n** (m, 4H), 1.49 **g** (t, 12H), 1.20 **o/p** (m, 8H).

3b, [1-H₂C(24C6)₂][BF₄]₂

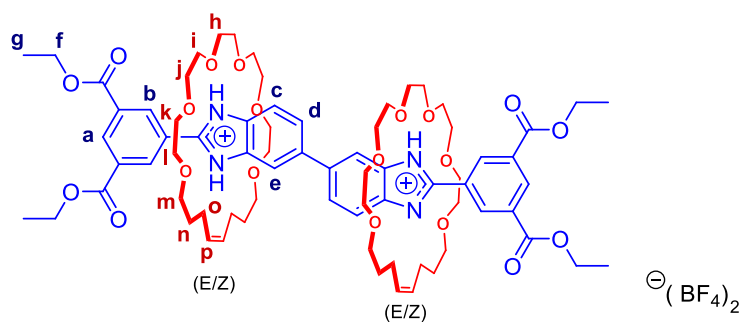


Figure 51. Structure and proton environments of **3b**

¹H NMR (500 MHz, CDCl₃): δ = 14.07 NH (s, 2H), 13.80 NH (s, 2H), 9.22 **b** (s, 4H), 9.17 **b'** (s, 2H), 8.95 **a** (s, 2H), 8.42 **c** (d, 2H, J = 8.5 Hz), 8.34 **e** (s, 2H), 8.19 **d** (d, 2H, J = 8.5 Hz), 5.07 **p** (s, 2H), 4.71 **p'** (s, 2H), 4.55 **f** (q, 8H, J = 7.0 Hz) 4.53, 4.04 **j/h** (m, 16H), 3.89 **k** (m, 8H), 3.73 **i** (m, 8H), 3.38 **l** (m, 8H), 2.89 **m** (m, 8H), 1.74 **n** (m, 8H), 1.49 **g** (t, 12H, J = 7.0 Hz) 1.49, 1.20 **o/p** (m, 16H).

3.5 Synthesis of 4a and 4b

4a

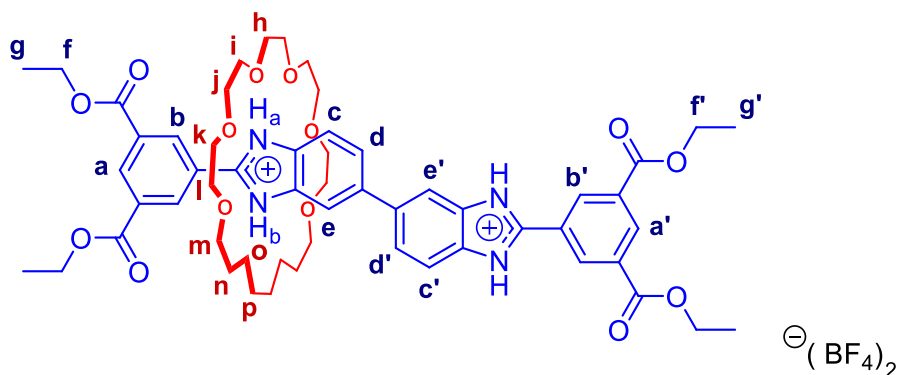


Figure 52. Structure and proton environments of **4a**.

Pd/C 10% w/w (35 mg, 0.33 mmol) was weighed into a 50 mL Schlenk flask and purge and backfilled with N₂. 20 mL of MeOH and 5 mL THF was used to dissolve and transfer **3a** (0.18 g, 0.16 mmol) to the flask under N₂. Vacuum was applied to the reaction flask until solvent was observed to boil. The reaction vessel was left until static vacuum and open to H₂(g) *via* a gas adapter and H₂ filled balloon. The reaction mixture was allowed to stir for 9 h after which mixture was filtered through Celite. The Celite was washed with CHCl₃ and the filtrate solvent was removed *via* a rotary evaporator. The residue was filtered using Et₂O to yield a white solid (110 mg, 70%), M.P Decomposition > 225°C.

¹H NMR (500 MHz, CDCl₃-d₁): δ = 13.95 **NH_b** (s, 1H), 13.53 **NH_a** (s, 1H), 9.17 **b'** (s, 2H), 9.13 **b** (d, 2H, J = 1.5 Hz), 9.03 **a'** (s, 1H), 8.98 **a** (d, 1H, J = 1.5 Hz), 8.65 **e'** (s, 1H), 8.34 **c'** (d, 1H, J = 8.5 Hz), 8.19 **e** (s, 1H), 8.00 **d** (d, 1H, J = 8.5 Hz), 7.88 **d'** (d, 1H, J = 8.5 Hz), 7.83 **c** (d, 1H, J = 8.5 Hz), 4.54 **f/f'** (qq, 8H, J = 7.0 Hz), 4.02 **j** (m, 4H), 3.93 **h** (m, 4H), 3.71 **k** (m,

4H), 3.45 **i** (m,4H), 3.35 **l** (m, 4H), 2.92 **m** (m,4H), 1.52 **g** (t, 12H, J= 7.0 Hz), 1.19 (m, 4H), 0.83 **o/p** (m, 8H).

¹³C NMR (126 MHz, CDCl₃-d₁) δ = 164.58, 164.41, 148.00, 147.49, 139.81, 138.59, 135.79, 134.64, 133.66, 133.57, 132.52, 132.49, 132.46, 132.15, 131.72, 130.70, 127.11, 126.72, 124.45, 122.55, 116.35, 114.30, 114.26, 113.09, 100.18, 77.80, 77.48, 77.43, 77.23, 76.98, 72.25, 71.75, 71.50, 71.35, 70.92, 70.64, 62.70, 62.52, 29.59, 28.28, 25.32, 14.70, 14.22.

4b

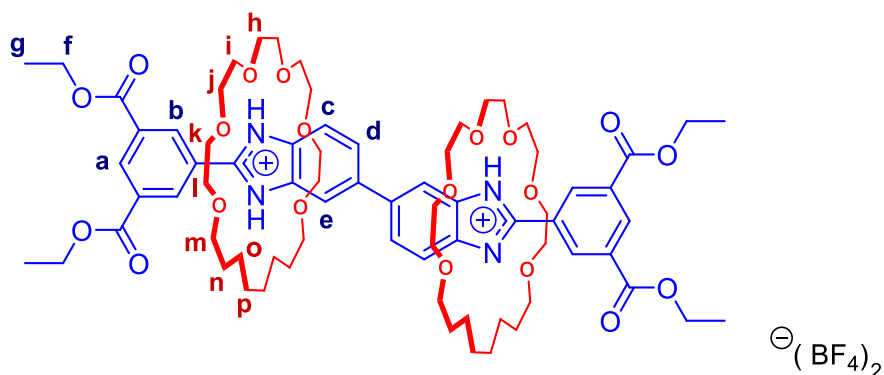


Figure 53. Structure and proton environment of **4b**.

Pd/C 10% w/w (15 mg, 0.14 mmol) was weighed into a 50 mL Schlenk flask and purge and backfilled with N₂. 15 mL of MeOH was used to dissolve and transfer **3b** (0.096 g, 0.07 mmol) to the flask under N₂. Vacuum was applied to the reaction flask until solvent was observed to boil. The reaction vessel was left under static vacuum and opened to H₂(g) *via* a gas adapter and H₂ filled balloon. The reaction mixture was allowed to stir for 8 h after which the mixture was filtered through Celite. The Celite was washed with CHCl₃ and the solvent was removed *via* rotary evaporator. The residue was filtered using Et₂O to yield a white solid (58 mg, 60%), M.P > 250°C (Dec.)

^1H NMR (500 MHz, CDCl_3): δ = 13.94 **NH** (s, 2H), 13.65 **NH** (s, 2H), 9.19 **b** (d, 4H, J = 1.5 Hz), 8.96 **a** (t, 2H, J = 1.5 Hz), 8.43 **c** (d, 2H, J = 8.5 Hz), 8.36 **e** (s, 2H), 8.21 **d** (d, 2H, J = 8.5 Hz), 4.01 **f** (q, 8H, J = 7.5 Hz), 3.70 **j/h** (m, 16H), 3.43 **k** (m, 8H), 3.26 **l/m** (m, 16H), 1.50 **g** (t, 12H, J = 7.5 Hz), 1.18 **n** (m, 8H), 0.83 **o/p** (m, 16H).

^{13}C NMR (126 MHz, CDCl_3): δ = 164.57, 147.11, 138.91, 134.20, 133.75, 132.02, 131.76, 130.84, 128.35, 124.74, 115.49, 112.06, 71.92, 71.36, 71.25, 71.02, 70.78, 70.58, 62.14, 29.46, 28.11, 25.14, 14.51

3.6 Synthesis of 5a and 5b

5a

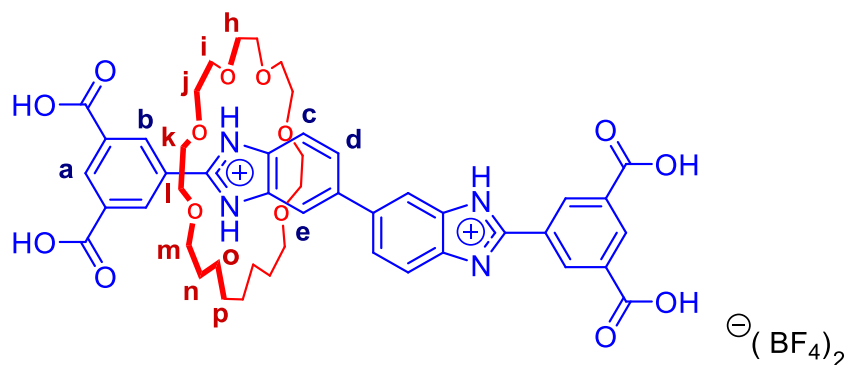


Figure 54. Structure and proton environment of **5a**

20 mL of EtOH was used to transfer **4a** (110mg, 0.1 mmol) to a Schlenk flask. 20 mL of 1M NaOH was added dropwise to the stirring solution. The reaction mixture was then allowed to reflux for 24 h. The non-aqueous solution was removed by rotary evaporator. The remaining aqueous solution was acidified to pH 5 with HBF₄ to give a gel suspension. The mixture was sonicated for 5 minutes and centrifuged for 20 mins. The pellet was sonicated in 10 mL water and centrifuged for an additional 20 mins. The supernatant was decanted and the pellet was sonicated in Et₂O and centrifuged for 20 mins. The pellet was left to air dry overnight to which a small amount of Et₂O was used to filter a light brown solid (77 mg, 78%) M.P. > 300°C (Dec.)

¹H NMR (500 MHz, DMSO-d₆): δ = 13.45 OH(s(broad), 4H) , 12.91 NH(s(broad), 2H), 9.09 **b**(s, 4H), 8.54 **a**(s,2H), 8.07 **e** (s(broad), 2H), 7.81 **c**(d(broad), 2H), 7.65(d(broad),2H), 3.33 **h/i/j/k/l/m** (m(broad), 24H), 1.34 **n**(m(broad), 4H), 1.10 **o/p** (m(broad), 8H)

^{13}C NMR (126 MHz, DMSO- d_6): δ = 166.85, 132.37, 132.1, 132.0, 131.9, 131.3, 131.1, 91.65, 80.1, 79.6, 79.4, 79.17, 71.02, 70.5, 69.9, 69.7, 69.0, 68.8, 29.1, 28.9, 25.5.

5b

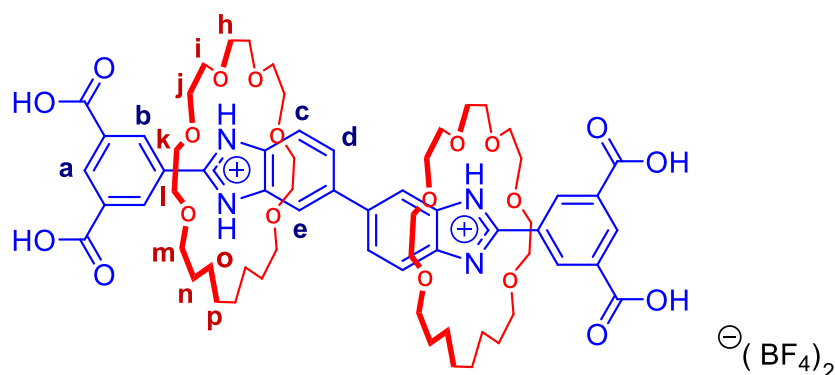


Figure 55. Structure and proton environments of **5b**.

20 mL of EtOH was used to transfer **4b** (58 mg, 0.1 mmol) to a Schlenk flask. 20 mL of 1M NaOH was added dropwise to the stirring solution. The reaction mixture was then allowed to reflux for 24 h. The non-aqueous solution was removed by rotary evaporator. The remaining aqueous solution was acidified to pH 4-5 with HBF_4 to precipitate a white solid. The suspension was centrifuged for 20 mins to which the pellet was sonicated in 10 mL acetone and centrifuged for an additional 15 mins. The pellet was left to air dry overnight in a pre-weighed vial to yield a white solid (35 mg, 53%) M.P > 300°C (Dec.).

^1H NMR (500 MHz, DMSO- d_6): δ = 13.82 **NH** (s(broad), 2H), 9.08 **b**(s, 4H), 8.79 **a** (s, 2H), 8.33 **e** (s, 2H), 8.18 **c/d** (m(broad), 4H), 3.60 **h/i/j/k/l/m** (m(broad), 48H), 1.13 **n** (m(broad), 8H), 0.80 **o/p** (m(broad), 16H).

3.7 Synthesis of Benzoic Acid Terminated Bis(benzimidazole) Axle

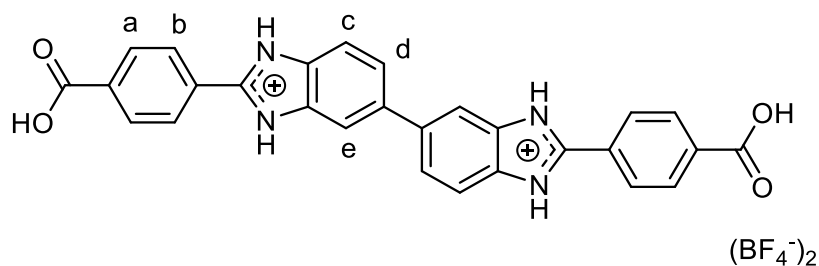


Figure 56. Structure and proton environments of benzoic acid terminated bis(benzimidazolium) axle.

1,4-benzoic acid (0.490 g, 2.3 mmol) and 3,3'-diamino benzidine (0.100 g, 0.47 mmol) were added to 1 g of polyphosphoric acid and heated at 180°C for 20 h. Reaction mixture was poured into water to yield a yellow precipitate. The solution was sonicated for 10 min and filtered hot. The crude solid was washed, sonicate and filtered hot in MeOH to yield a yellow solid (35 mg, 53%) M.P > 300°C (Dec.)

¹H NMR (500 MHz, DMSO-d₆): δ = 8.34 **a** (d, 4H, J = 8.5 Hz), 8.14 **b** (d, 4H, J = 8.5 Hz), 7.92 **e** (s, 2H), 7.76 **c** (d, 2H, J = 8.5 Hz), 7.65 **d** (d, 2H, J = 8.5 Hz)

¹³C NMR (126 MHz, DMSO-d₆): δ = 167.50, 162.87, 151.21, 136.66, 134.35, 132.13, 130.49, 127.02, 122.97

References

- (1) Meng, Z.; Xiang, J.-F.; Chen, C.-F. Tristable [n]rotaxanes: from molecular shuttle to molecular cable car. *Chem. Sci.* **2014**, 5 (4), 1520.
- (2) Zhu, K.; Vukotic, V. N.; Noujeim, N.; Loeb, S. J. Bis(benzimidazolium) axles and crown ether wheels: a versatile templating pair for the formation of [2]rotaxane molecular shuttles. *Chem. Sci.* **2012**, 3 (11), 3265.
- (3) Cao, Z.-Q.; Li, H.; Yao, J.; Zou, L.; Qu, D.-H.; Tian, H. A Perylene-Bridged Switchable [3]Rotaxane Molecular Shuttle with a Fluorescence Output. *Asian J. Org. Chem.* **2015**, 4 (3), 212–216.
- (4) Davidson, G. J. E.; Sharma, S.; Loeb, S. J. A [2]Rotaxane Flip Switch Driven by Coordination Geometry. *Angew. Chemie-Int. Ed.* **2010**, 49 (29), 4938–4942.
- (5) Loeb, S. J.; Tiburcio, J.; Vella, S. J. A mechanical "flip-switch". Interconversion between co-conformations of a 2 rotaxane with a single recognition site. *Chem. Commun.* **2006**, No. 15, 1598–1600.
- (6) Coskun, A.; Wesson, P. J.; Klajn, R.; Trabolsi, A.; Fang, L.; Olson, M. A.; Dey, S. K.; Grzybowski, B. A.; Stoddart, J. F. Molecular-Mechanical Switching at the Nanoparticle-Solvent Interface: Practice and Theory. *J. Am. Chem. Soc.* **2010**, 132 (12), 4310–4320.
- (7) Leigh, D. A.; Wong, J. K. Y.; Dehez, F.; Zerbetto, F. Unidirectional rotation in a mechanically interlocked molecular rotor. *Nature* **2003**, 424 (6945), 174–179.
- (8) Kay, E. R.; Leigh, D. A.; Zerbetto, F. Synthetic molecular motors and mechanical machines. *Angew. Chemie-Int. Ed.* **2007**, 46 (1-2), 72–191.

- (9) Farahani, N.; Zhu, K.; Noujeim, N.; Loeb, S. J. [2]Pseudorotaxane formation between rigid Y-shaped 2,4,5-triphenylimidazolium axles and [24]crown-8 ether wheels. *Org. Biomol. Chem.* **2014**, *12* (27), 4824–4827.
- (10) Jimenez, R.; Martin, C.; Lopez-Cornejo, P. Formation of a rotaxane from the end-capping process of a pseudorotaxane. Effects of the solvent. *J. Phys. Chem. B* **2008**, *112* (37), 11610–11615.
- (11) Vukotic, V. N.; Harris, K. J.; Zhu, K.; Schurko, R. W.; Loeb, S. J. Metal–organic frameworks with dynamic interlocked components. *Nat. Chem.* **2012**, *4* (6), 456–460.
- (12) Mercer, D. J.; Yacoub, J.; Zhu, K.; Loeb, S. K.; Loeb, S. J. [2]Pseudorotaxanes, [2]rotaxanes and metal–organic rotaxane frameworks containing tetra-substituted dibenzo[24]crown-8 wheels. *Org. Biomol. Chem.* **2012**, *10* (30), 6094.
- (13) Coskun, A.; Banaszak, M.; Astumian, R. D.; Stoddart, J. F.; Grzybowski, B. a. Great expectations: can artificial molecular machines deliver on their promise? *Chem. Soc. Rev.* **2012**, *41* (1), 19.
- (14) Zhu, K.; Vukotic, V. N.; Loeb, S. J. Molecular shuttling of a compact and rigid H-shaped [2]rotaxane. *Angew. Chemie - Int. Ed.* **2012**, *51* (9), 2168–2172.
- (15) Loeb, S. J.; Tiburcio, J.; Vella, S. J. 2 Pseudorotaxane formation with N-benzylanilinium axles and 24-crown-8 ether wheels. *Org. Lett.* **2005**, *7* (22), 4923–4926.
- (16) Bissell, R. A.; Cordova, E.; Kaifer, A. E.; Stoddart, J. F. A Chemically and Electrochemically Switchable Molecular Shuttle. *Nature* **1994**, *369* (6476),

133–137.

- (17) Nygaard, S.; Leung, K. C. F.; Aprahamian, I.; Ikeda, T.; Saha, S.; Laursen, B. W.; Kim, S.-Y.; Hansen, S. W.; Stein, P. C.; Flood, A. H.; et al. Functionally rigid bistable 2 rotaxanes. *J. Am. Chem. Soc.* **2007**, *129* (4), 960–970.
- (18) Ashton, P. R.; Ballardini, R.; Balzani, V.; Credi, A.; Dress, K. R.; Ishow, E.; Kleverlaan, C. J.; Kocian, O.; Preece, J. A.; Spencer, N.; et al. A photochemically driven molecular-level abacus. *Chem. Eur. J.* **2000**, *6* (19), 3558–3574.
- (19) Li, H.; Eddaoudi, M.; O’Keeffe, M.; Yaghi, O. M. Design and synthesis of an exceptionally stable and highly porous metal-organic framework. *Nature* **1999**, *402* (11), 276–279.
- (20) Chui, S. S.-Y.; Lo, S. M.-F.; Charmant, J. P. H.; Orpen, A. G.; Williams, I. D. A Chemically Functionalizable Nanoporous Material $[\text{Cu}_3(\text{TMA})_2(\text{H}_2\text{O})_3]_n$. *Science* **1999**, *283* (5405).
- (21) Chun, H.; Dybtsev, D. N.; Kim, H.; Kim, K. Synthesis, X-ray crystal structures, and gas sorption properties of pillared square grid nets based on paddle-wheel motifs: Implications for hydrogen storage in porous materials. *Chem. - A Eur. J.* **2005**, *11* (12), 3521–3529.
- (22) Eddaoudi, M.; Moler, D. B.; Li, H.; Chen, B.; Reineke, T. M.; O’Keeffe, M.; Yaghi, O. M. Modular chemistry: Secondary building units as a basis for the design of highly porous and robust metal-organic carboxylate frameworks. *Acc. Chem. Res.* **2001**, *34* (4), 319–330.
- (23) Hoffart, D. J.; Loeb, S. J. The missing link: A 2D metal-organic rotaxane framework (MORF) with one rotaxane linker and one naked linker. *Supramol.*

Chem. **2007**, *19* (1-2), 89–93.

- (24) Davidson, G. J. E.; Loeb, S. J. Channels and cavities lined with interlocked components: Metal-based polyrotaxanes that utilize pyridinium axles and crown ether wheels as ligands. *Angew. Chemie-Int. Ed.* **2003**, *42* (1), 74–77.
- (25) Hoffart, D. J.; Loeb, S. J. Metal-organic rotaxane frameworks: Three-dimensional polyrotaxanes from lanthanide-ion nodes, pyridinium N-oxide axles, and crown-ether wheels. *Angew. Chemie-Int. Ed.* **2005**, *44* (6), 901–904.
- (26) Jeon, W. S.; Moon, K.; Park, S. H.; Chun, H.; Ko, Y. H.; Lee, J. Y.; Lee, E. S.; Samal, S.; Selvapalam, N.; Rekharsky, M. V.; et al. Complexation of ferrocene derivatives by the cucurbit[7]uril host: A comparative study of the cucurbituril and cyclodextrin host families. *J. Am. Chem. Soc.* **2005**, *127* (37), 12984–12989.
- (27) Whang, D.; Kim, K. Polycatenated two-dimensional polyrotaxane net. *J. Am. Chem. Soc.* **1997**, *119* (2), 451–452.
- (28) Lee, E. S.; Heo, J. S.; Kim, K. A three-dimensional polyrotaxane network. *Angew. Chemie-Int. Ed.* **2000**, *39* (15), 2699–2701.
- (29) Eddaoudi, M.; Kim, J.; Rosi, N.; Vodak, D.; Wachter, J.; O’Keeffe, M.; Yaghi, O. M. Systematic design of pore size and functionality in isorecticular MOFs and their application in methane storage. *Science* **2002**, *295* (5554), 469–472.
- (30) Kim, K. Mechanically interlocked molecules incorporating cucurbituril and their supramolecular assemblies. *Chem Soc Rev* **2002**, *31* (2), 96–107.
- (31) Whang, D.; Heo, J.; Kim, C. A.; Kim, K. Helical polyrotaxane: cucurbituril “beads” threaded onto a helical one-dimensional coordination polymer. *Chem. Commun.* **1997**, No. 24, 2361–2362.

- (32) Deng, H.; Olson, M. A.; Stoddart, J. F.; Yaghi, O. M. Robust dynamics. *Nat Chem* **2010**, 2 (6), 439–443.
- (33) Noujeim, N.; Zhu, K.; Vukotic, V. N.; Loeb, S. J. Pseudorotaxanes from T-shaped benzimidazolium axles and [24]crown-8 wheels. *Org. Lett.* **2012**, 14 (10), 2484–2487.
- (34) Li, C. Q.; Qiu, W. G.; Shi, W.; Song, H. B.; Bai, G. M.; He, H.; Li, J.; Zaworotko, M. J. A pcu-type metal-organic framework based on covalently quadruple cross-linked supramolecular building blocks (SBBs): structure and adsorption properties. *Cryst. Eng. Comm.* **2012**, 14 (6), 1929–1932.
- (35) Wang, X. S.; Ma, S. Q.; Forster, P. M.; Yuan, D. Q.; Eckert, J.; Lopez, J. J.; Murphy, B. J.; Parise, J. B.; Zhou, H. C. Enhancing H₂ uptake by “Close-Packing” alignment of open copper sites in metal-organic frameworks. *Angew. Chemie-Int. Ed.* **2008**, 47 (38), 7263–7266.
- (36) Lin, X.; Telepeni, I.; Blake, A. J.; Dailly, A.; Brown, C. M.; Simmons, J. M.; Zoppi, M.; Walker, G. S.; Thomas, K. M.; Mays, T. J.; et al. High Capacity Hydrogen Adsorption in Cu(II) Tetracarboxylate Framework Materials: The Role of Pore Size, Ligand Functionalization, and Exposed Metal Sites. *J. Am. Chem. Soc.* **2009**, 131 (6), 2159–2171.
- (37) Vukotic, V. N. Mechanically Interlocked Linkers for Dynamic Metal-Organic Frameworks, University of Windsor, 2014.
- (38) Geng, J.; Tao, T.; Chen, H.-Q.; Huang, W. The first observation of cis and trans isomers for bibenzo[d]imidazole-based compounds influenced by halogen substituent effects. *Inorg. Chem. Commun.* **2014**, 42, 23–28.

- (39) Saha, S.; Ravikumar, I.; Ghosh, P. A Fluorophoric-Axle-Based, Nonfluorescent, Metallo anti-[3]Pseudorotaxane: Recovery of Fluorescence by Means of an Axle Substitution Reaction. *Chem. - A Eur. J.* **2011**, *17* (49), 13712–13719.
- (40) Chesman, A. S. R.; Turner, D. R.; Price, D. J.; Moubaraki, B.; Murray, K. S.; Deacon, G. B.; Batten, S. R. Solvothermal vs. bench-top reactions: Control over the formation of discrete complexes and coordination polymers. *Chem. Commun.* **2007**, *2* (34), 3541.
- (41) Dy, J. T.; Ogawa, K.; Satake, A.; Ishizumi, A.; Kobuke, Y. Water-soluble self-assembled butadiyne-bridged bisporphyrin: A potential two-photon-absorbing photosensitizer for photodynamic therapy. *Chem. Eur. J.* **2007**, *13* (12), 3491–3500.
- (42) Kilbinger, A. F. M.; Cantrill, S. J.; Waltman, A. W.; Day, M. W.; Grubbs, R. H. Magic ring rotaxanes by olefin metathesis. *Angew. Chemie-Int. Ed.* **2003**, *42* (28), 3281–3285.

Appendix

Copyright Permissions



RightsLink®

Home

Account
Info

Help

L



Taylor & Francis
Taylor & Francis Group

Title:

The Missing Link: A 2D Metal-Organic Rotaxane Framework (MORF) with One Rotaxane Linker and One Naked Linker

Author:

Dennis J. Hoffart, Stephen J. Loeb

Publication: Supramolecular Chemistry

Publisher: Taylor & Francis

Date: Mar 1, 2007

Copyright © 2007 Taylor & Francis

Logged in as:

Christine To

LOGOUT

Thesis/Dissertation Reuse Request

Taylor & Francis is pleased to offer reuses of its content for a thesis or dissertation free of charge contingent on resubmission of permission request if work is published.



Title: Channels and Cavities Lined with Interlocked Components: Metal-Based Polyrotaxanes That Utilize Pyridinium Axles and Crown Ether Wheels as Ligands

Author: Gregory J. E. Davidson, Stephen J. Loeb

Publication: Angewandte Chemie International Edition

Publisher: John Wiley and Sons

Date: Jan 3, 2003

Copyright © 2003 WILEY-VCH Verlag GmbH & Co. KGaA, Weinheim

Logged in as:

Christine To

LOGOUT

Order Completed

Thank you for your order.

This Agreement between Christine To ("You") and John Wiley and Sons ("John Wiley and Sons") consists of your license details and the terms and conditions provided by John Wiley and Sons and Copyright Clearance Center.

Your confirmation email will contain your order number for future reference.

[Get the printable license.](#)

License Number	3878401186419
License date	May 29, 2016
Licensed Content Publisher	John Wiley and Sons
Licensed Content Publication	Angewandte Chemie International Edition
Licensed Content Title	Channels and Cavities Lined with Interlocked Components: Metal-Based Polyrotaxanes That Utilize Pyridinium Axles and Crown Ether Wheels as Ligands
Licensed Content Author	Gregory J. E. Davidson, Stephen J. Loeb
Licensed Content Date	Jan 3, 2003
Licensed Content Pages	4
Type of use	Dissertation/Thesis
Requestor type	University/Academic
Format	Print and electronic
Portion	Figure/table
Number of figures/tables	1
Original Wiley figure/table number(s)	Figure 4
Will you be translating?	No
Title of your thesis / dissertation	Bisbenzimidazolium Rotaxane Molecular Shuttles
Expected completion date	Jun 2016
Expected size (number of pages)	82
Requestor Location	Christine To 2288 Amy Lynn Park Drive Windsor, ON N9E 4N3 Canada Attn: Christine To
Billing Type	Invoice
Billing address	Christine To 2288 Amy Lynn Park Drive Windsor, ON N9E 4N3 Canada Attn: Christine To
Total	0.00 USD



Title: Metal-Organic Rotaxane Frameworks: Three-Dimensional Polyrotaxanes from Lanthanide-Ion Nodes, Pyridinium N-Oxide Axles, and Crown-Ether Wheels

Author: Dennis J. Hoffart, Stephen J. Loeb

Publication: Angewandte Chemie International Edition

Publisher: John Wiley and Sons

Date: Dec 28, 2004

Copyright © 2005 WILEY-VCH Verlag GmbH & Co. KGaA, Weinheim

Logged in as:
Christine To

LOGOUT

Order Completed

Thank you for your order.

This Agreement between Christine To ("You") and John Wiley and Sons ("John Wiley and Sons") consists of your license details and the terms and conditions provided by John Wiley and Sons and Copyright Clearance Center.

Your confirmation email will contain your order number for future reference.

[Get the printable license.](#)

License Number	3878401361532
License date	May 29, 2016
Licensed Content Publisher	John Wiley and Sons
Licensed Content Publication	Angewandte Chemie International Edition
Licensed Content Title	Metal-Organic Rotaxane Frameworks: Three-Dimensional Polyrotaxanes from Lanthanide-Ion Nodes, Pyridinium N-Oxide Axles, and Crown-Ether Wheels
Licensed Content Author	Dennis J. Hoffart, Stephen J. Loeb
Licensed Content Date	Dec 28, 2004
Licensed Content Pages	4
Type of use	Dissertation/Thesis
Requestor type	University/Academic
Format	Print and electronic
Portion	Figure/table
Number of figures/tables	2
Original Wiley figure/table number(s)	Figure 2
Will you be translating?	No
Title of your thesis / dissertation	Bisbenzimidazolium Rotaxane Molecular Shuttles
Expected completion date	Jun 2016
Expected size (number of pages)	82
Requestor Location	Christine To 2288 Amy Lynn Park Drive Windsor, ON N9E 4N3 Canada Attn: Christine To
Billing Type	Invoice
Billing address	Christine To 2288 Amy Lynn Park Drive Windsor, ON N9E 4N3 Canada Attn: Christine To
Total	0.00 USD



Title: Design and synthesis of an exceptionally stable and highly porous metal-organic framework

Author: Hailian Li, Mohamed Eddaoudi, M. O'Keeffe and O. M. Yaghi

Publication: Nature

Publisher: Nature Publishing Group

Date: Nov 18, 1999

Copyright © 1999, Rights Managed by Nature Publishing Group

Logged in as:
Christine To

LOGOUT

Order Completed

Thank you very much for your order.

This is a License Agreement between Christine To ("You") and Nature Publishing Group ("Nature Publishing Group"). The license consists of your order details, the terms and conditions provided by Nature Publishing Group, and the [payment terms and conditions](#).

[Get the printable license.](#)

License Number	3878391262412
License date	May 29, 2016
Licensed content publisher	Nature Publishing Group
Licensed content publication	Nature
Licensed content title	Design and synthesis of an exceptionally stable and highly porous metal-organic framework
Licensed content author	Hailian Li, Mohamed Eddaoudi, M. O'Keeffe and O. M. Yaghi
Licensed content date	Nov 18, 1999
Type of Use	reuse in a dissertation / thesis
Volume number	402
Issue number	6759
Requestor type	academic/educational
Format	print and electronic
Portion	figures/tables/illustrations
Number of figures/tables/illustrations	1
Figures	Figure 1
Author of this NPG article	no
Your reference number	None
Title of your thesis / dissertation	Bisbenzimidazolium Rotaxane Molecular Shuttles
Expected completion date	Jun 2016
Estimated size (number of pages)	82
Total	0.00 USD



Title: A Chemically Functionalizable Nanoporous Material $[\text{Cu}_3(\text{TMA})_2(\text{H}_2\text{O})_3]_n$

Author: Stephen S.-Y. Chui, Samuel M.-F. Lo, Jonathan P. H. Charmant, A. Guy Orpen, Ian D. Williams

Logged in as:
Christine To

LOGOUT

Publication: Science

Publisher: The American Association for the Advancement of Science

Date: Feb 19, 1999

Copyright © 1999, The American Association for the Advancement of Science

Order Completed

Thank you very much for your order.

This is a License Agreement between Christine To ("You") and The American Association for the Advancement of Science ("The American Association for the Advancement of Science"). The license consists of your order details, the terms and conditions provided by The American Association for the Advancement of Science, and the [payment terms and conditions](#).

[Get the printable license.](#)

License Number	3878400006514
License date	May 29, 2016
Licensed content publisher	The American Association for the Advancement of Science
Licensed content publication	Science
Licensed content title	A Chemically Functionalizable Nanoporous Material $[\text{Cu}_3(\text{TMA})_2(\text{H}_2\text{O})_3]_n$
Licensed content author	Stephen S.-Y. Chui, Samuel M.-F. Lo, Jonathan P. H. Charmant, A. Guy Orpen, Ian D. Williams
Licensed content date	Feb 19, 1999
Volume number	283
Issue number	5405
Type of Use	Thesis / Dissertation
Requestor type	Scientist/individual at a research institution
Format	Print and electronic
Portion	Figure
Number of figures/tables	1
Order reference number	None
Title of your thesis / dissertation	Bisbenzimidazolium Rotaxane Molecular Shuttles
Expected completion date	Jun 2016
Estimated size(pages)	82
Total	0.00 USD



RightsLink®

[Home](#)

[Account Info](#)

[Help](#)



ACS Publications
Most Trusted. Most Cited. Most Read.

Title: Polycatenated Two-Dimensional Polyrotaxane Net
Author: Dongmok Whang, Kimoon Kim
Publication: Journal of the American Chemical Society
Publisher: American Chemical Society
Date: Jan 1, 1997
Copyright © 1997, American Chemical Society

Logged in as:
Christine To

[LOGOUT](#)

PERMISSION/LICENSE IS GRANTED FOR YOUR ORDER AT NO CHARGE

This type of permission/license, instead of the standard Terms & Conditions, is sent to you because no fee is being charged for your order. Please note the following:

- Permission is granted for your request in both print and electronic formats, and translations.
- If figures and/or tables were requested, they may be adapted or used in part.
- Please print this page for your records and send a copy of it to your publisher/graduate school.
- Appropriate credit for the requested material should be given as follows: "Reprinted (adapted) with permission from (COMPLETE REFERENCE CITATION). Copyright (YEAR) American Chemical Society." Insert appropriate information in place of the capitalized words.
- One-time permission is granted only for the use specified in your request. No additional uses are granted (such as derivative works or other editions). For any other uses, please submit a new request.



Title: A Three-Dimensional Polyrotaxane Network
Author: Eunsung Lee, Jungseok Heo, Kimoon Kim
Publication: Angewandte Chemie International Edition
Publisher: John Wiley and Sons
Date: Aug 2, 2000
 © 2000 WILEY-VCH Verlag GmbH, Weinheim, Fed. Rep. of Germany

Logged in as:
Christine To

LOGOUT

Order Completed

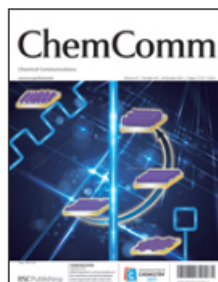
Thank you for your order.

This Agreement between Christine To ("You") and John Wiley and Sons ("John Wiley and Sons") consists of your license details and the terms and conditions provided by John Wiley and Sons and Copyright Clearance Center.

Your confirmation email will contain your order number for future reference.

[Get the printable license.](#)

License Number	3878420882221
License date	May 29, 2016
Licensed Content Publisher	John Wiley and Sons
Licensed Content Publication	Angewandte Chemie International Edition
Licensed Content Title	A Three-Dimensional Polyrotaxane Network
Licensed Content Author	Eunsung Lee, Jungseok Heo, Kimoon Kim
Licensed Content Date	Aug 2, 2000
Licensed Content Pages	3
Type of use	Dissertation/Thesis
Requestor type	University/Academic
Format	Print and electronic
Portion	Figure/table
Number of figures/tables	1
Original Wiley figure/table number(s)	Scheme 1
Will you be translating?	No
Title of your thesis / dissertation	Bisbenzimidazolium Rotaxane Molecular Shuttles
Expected completion date	Jun 2016
Expected size (number of pages)	82
Requestor Location	Christine To 2288 Amy Lynn Park Drive Windsor, ON N9E 4N3 Canada Attn: Christine To
Billing Type	Invoice
Billing address	Christine To 2288 Amy Lynn Park Drive Windsor, ON N9E 4N3 Canada Attn: Christine To
Total	0.00 USD



Title: Helical polyrotaxane: cucurbituril 'beads' threaded onto a helical one-dimensional coordination polymer
Author: Dongmok Whang, Kimoon Kim
Publication: Chemical Communications (Cambridge)
Publisher: Royal Society of Chemistry
Date: Dec 31, 1969
Copyright © 1969, Royal Society of Chemistry

Logged in as:
Christine To

LOGOUT

Order Completed

Thank you for your order.

This Agreement between Christine To ("You") and Royal Society of Chemistry ("Royal Society of Chemistry") consists of your license details and the terms and conditions provided by Royal Society of Chemistry and Copyright Clearance Center.

Your confirmation email will contain your order number for future reference.

[Get the printable license.](#)

License Number	3878421307682
License date	May 29, 2016
Licensed Content Publisher	Royal Society of Chemistry
Licensed Content Publication	Chemical Communications (Cambridge)
Licensed Content Title	Helical polyrotaxane: cucurbituril 'beads' threaded onto a helical one-dimensional coordination polymer
Licensed Content Author	Dongmok Whang, Kimoon Kim
Licensed Content Date	Dec 31, 1969
Licensed Content Issue	24
Type of Use	Thesis/Dissertation
Requestor type	non-commercial (non-profit)
Portion	figures/tables/images
Number of figures/tables/images	1
Distribution quantity	4
Format	print and electronic
Will you be translating?	no
Order reference number	None
Title of the thesis/dissertation	Bisbenzimidazolium Rotaxane Molecular Shuttles
Expected completion date	Jun 2016
Estimated size	82
Requestor Location	Christine To 2288 Amy Lynn Park Drive Windsor, ON N9E 4N3 Canada Attn: Christine To
Billing Type	Invoice
Billing address	Christine To 2288 Amy Lynn Park Drive Windsor, ON N9E 4N3 Canada Attn: Christine To
Total	0.00 USD



Title: A molecular shuttle that operates inside a metal-organic framework

Author: Kelong Zhu, Christopher A. O'Keefe, V. Nicholas Vukotic, Robert W. Schurko, Stephen J. Loeb

Publication: Nature Chemistry

Publisher: Nature Publishing Group

Date: May 4, 2015

Copyright © 2015, Rights Managed by Nature Publishing Group

Logged in as:
Christine To

[LOGOUT](#)

Order Completed

Thank you very much for your order.

This is a License Agreement between Christine To ("You") and Nature Publishing Group ("Nature Publishing Group"). The license consists of your order details, the terms and conditions provided by Nature Publishing Group, and the [payment terms and conditions](#).

[Get the printable license.](#)

License Number	3878430067608
License date	May 29, 2016
Licensed content publisher	Nature Publishing Group
Licensed content publication	Nature Chemistry
Licensed content title	A molecular shuttle that operates inside a metal-organic framework
Licensed content author	Kelong Zhu, Christopher A. O'Keefe, V. Nicholas Vukotic, Robert W. Schurko, Stephen J. Loeb
Licensed content date	May 4, 2015
Type of Use	reuse in a dissertation / thesis
Volume number	7
Issue number	6
Requestor type	academic/educational
Format	print and electronic
Portion	figures/tables/illustrations
Number of figures/tables/illustrations	1
High-res required	no
Figures	Figure 2
Author of this NPG article	no
Your reference number	None
Title of your thesis / dissertation	Bisbenzimidazolium Rotaxane Molecular Shuttles
Expected completion date	Jun 2016
Estimated size (number of pages)	82
Total	0.00 USD

Vita Auctoris

Name: Christine To

Year of Birth: 1992

Place of Birth: Windsor Ontario

Education: MSc. Chemistry (2016)
University of Windsor, Windsor, Ontario, Canada

BSc. Honours Chemistry with Thesis (2014)
University of Windsor, Windsor, Ontario, Canada

Holy Names High School (2010)
Windsor, Ontario, Canada

Scholarships and Awards

Award	Year	Amount
NSERC CGS M	2015	\$17 500
Tri-Council Recognition Scholarship (TCRS)	2015	\$5 000
Ontario Graduate Scholarship	2014	\$15 000